Chapter 1
Instruments for Measuring Gravity

L. Vitushkin, L. Elinson, A. Krasnov, V. G. Peshekhonov, A. Sokolov, Yu. Smoller, and S. Yurist

Abstract This chapter describes technical instrumentation for gravity measurements. Various types of absolute ballistic gravimeters intended for ground-based measurements of the absolute free-fall acceleration are described. The focus is on the most recently used laser-interferometric absolute gravimeters. Regular international comparisons of absolute gravimeters are considered. Applications of ground-based absolute gravimetry using ballistic gravimeters for the national and international geodetic projects such as the Global Geodetic Observing System of the International Association of Geodesy are described. Development and operation of the Russian Chekan and GT-2 series mobile gravimeters are addressed.

Keywords Absolute ballistic gravimeters · International comparisons of absolute gravimeters · Relative gravimeters · Gravimeter Chekan · Gravimeter GT-2A

Introduction

This chapter is devoted to the description of the technical instrumentation for gravity measurement. It contains three sections.

L. Elinson—Deceased

L. Vitushkin
Mendeleyev Institute for Metrology, St. Petersburg, Russia

L. Elinson · A. Krasnov (✉) · V. G. Peshekhonov · A. Sokolov
Concern CSRI Elektropribor, St. Petersburg, Russia
e-mail: anton-krasnov@mail.ru

V. G. Peshekhonov
e-mail: onti@eprib.ru

A. Krasnov · V. G. Peshekhonov · A. Sokolov
ITMO University, St. Petersburg, Russia

Yu. Smoller · S. Yurist
Gravimetric Technologies, Moscow, Russia

V. G. Peshekhonov and O. A. Stepanov (eds.), *Methods and Technologies for Measuring the Earth's Gravity Field Parameters*, Earth Systems Data and Models 5,
https://doi.org/10.1007/978-3-031-11158-7_1

Section 1.1 describes the principle of operation, structure, and design features of various types of modern absolute ballistic gravimeters (ABG) intended for ground-based measurements of the absolute values of the free-fall acceleration (FFA). The focus is on the most recently used laser-interferometric ABGs, which determine FFA based on measurements—conducted with a laser displacement interferometer—of the travel path of a macroscopic test body (MTB) and the time intervals during its free fall in a gravitational field. The sources of uncertainties in FFA measurements using the ABGs are analyzed. The chapter provides an analysis of the modern metrological assurance system for absolute gravimeters. It is pointed out that, in order to determine ABG metrological characteristics belonging to national metrological institutes, regular international comparisons under the auspices of the International Committee of Weights and Measures and regional international comparisons are held under the authority of regional metrological organizations. The results of these comparisons are briefly described, also given is the information on the international database of absolute FFA measurements, developed by the Institute of Geodesy of the German Federal Agency for Cartography and Geodesy (BKG). Applications of ground-based absolute gravimetry using ABGs for the implementation of national and international projects in modern geodesy such as the Global Geodetic Observing System of the International Association of Geodesy are described. The section points out the current trend of research aimed at determining whether it is possible to carry out absolute FFA measurements using ABGs on moving platforms in marine and airborne gravimetry.

Sections 1.2 **and** 1.3 describe the features of the development and operation of the Russian Chekan series (Sect. 1.2) and GT-2 series (Sect. 1.3) mobile gravimeters. These systems belong to the class of relative gravimeters, i.e., those designed to measure gravity increments. They are widely used for high-precision measurements of the Earth's gravitational field from sea vessels and aircraft, including measurements in hard-to-reach Arctic and Antarctic areas.

Each section provides brief information on the development history of the instruments, describes design features of gravimeter sensing elements along with their block diagrams, and gives a detailed description of the main technical solutions implemented when building the latest versions of gravimeters. Mathematical models of gravity sensors and inertial sensing elements used are provided. The main structural features and the sources of uncertainties of stabilization and correction circuits for gyrostabilized platforms are analyzed.

1.1 Absolute Gravimeters

Absolute measurements of the free-fall acceleration (gravity) are the basis for the determination of the Earth's gravitational field (EGF). In absolute measurements, the measurement result is represented by the absolute FFA value, in contrast to relative measurements, the result of which is represented by the difference between FFA values at the stations where the measurements were taken.

At the initial stages of the development of instruments for measuring the gravitational field, the number of absolute FFA measurements was insignificant, and the uncertainties in measurements were relatively large.

From 1909 to 1971, all gravitational field measurements were performed in the framework of the Potsdam Gravimetric System. At the initial gravimetric site, absolute measurements were taken using reversible pendulums, and their uncertainty was 3 mGal (1 Gal = 1 cm/s^2) (Cook 1965).

IGSN-1971, the gravimetric system that combines gravitational field measurements throughout the world, was adopted by the General Assembly of the International Union of Geodesy and Geophysics in Moscow in 1971, Russia (Resolution 16).

IGSN-71 was originally based on 10 absolute measurements at 8 gravimetric sites with an FFA measurement uncertainty of 1 mGal.

In the 1970s, IGSN-1971 was expanded to 471 sites with 24,000 links measured using relative gravimeters and with 1200 absolute measurements using pendulum gravimeters. The uncertainty in the FFA determination was 0.1 mGal.

In 1986, G. Boedeker and T. Fritzer proposed a new International Absolute Gravity Basestation Network (IAGBN) within which the monitoring of variations in the gravitational field was to be carried out, but the intended set of sites was not implemented.

The emergence of transportable absolute ballistic gravimeters in the 1970s resulted in a significant increase in the accuracy of absolute FFA measurements, increasing their number, and made it possible to build a new global system of absolute gravimetric sites with an uncertainty in measuring absolute FFA values not exceeding 10 μGal.

It should be noted that the modern international database of absolute measurements AGrav developed and supported jointly by the German Federal Agency of Cartography and Geodesy and the International Gravimetric Bureau (BGI) (France) presents the results of more than 3300 absolute measurements by 50 absolute gravimeters with 1100 gravimetric sites (http://agrav.bkg.bund.de).

1.1.1 Types and Designs of Absolute Ballistic Gravimeters

At present, absolute FFA values can be measured by ABGs, in which laser interferometers measure the fall path of an MTB with an optical interferometer reflector attached to it or with cold atom interferometers for which the test objects are the clouds of cold atoms. The term “ballistic” is associated with the type of the free-fall path of the test body in a gravimeter. In such gravimeters, the free motion of the test body in the gravitational field is used, and the FFA is calculated from the measured path and time intervals from the test body ballistic motion equation (Cook 1965).

ABGs use two types of the test body trajectories: symmetric (a rise-and-fall trajectory such that the test body is thrown up and then falls down) and asymmetric (a free-fall trajectory such that the test body falls down freely). An example of a gravimeter with a symmetric trajectory is the device developed by the Italian National Institute of

Metrological Research (INRIM) (Germak et al. 2002). However, most of the modern ABGs have an asymmetric trajectory (please see Niebauer et al. 1995; Arnautov et al. 1974; Vitouchkine and Faller 2002; Vitushkin and Orlov 2014).

Figure 1.1 shows a schematic of a laser-interferometric ABG, which is implemented in various designs of gravimeters with an MTB, where a displacement laser interferometer is used to measure the free-fall trajectory.

At present, the relative uncertainty of the absolute FFA measurements using ABGs is about 10^{-9} (several microgal in absolute units). However, it should be noted that such a measurement uncertainty cannot be obtained in a single throw of the proof mass but is obtained in comparably long series of throws.

ABGs with an MTB normally include:

- a vacuum chamber with a ballistic unit, test body, and a vacuum system;
- a laser interferometer to measure the displacement of the test body in its free motion, passive or active vibration isolation system for the reference reflector, against which the laser interferometer measures the test body displacement;
- a frequency-stabilized laser of the laser interferometer;
- a path and time interval recording system, a reference rubidium frequency oscillator for the path and time interval recording system;

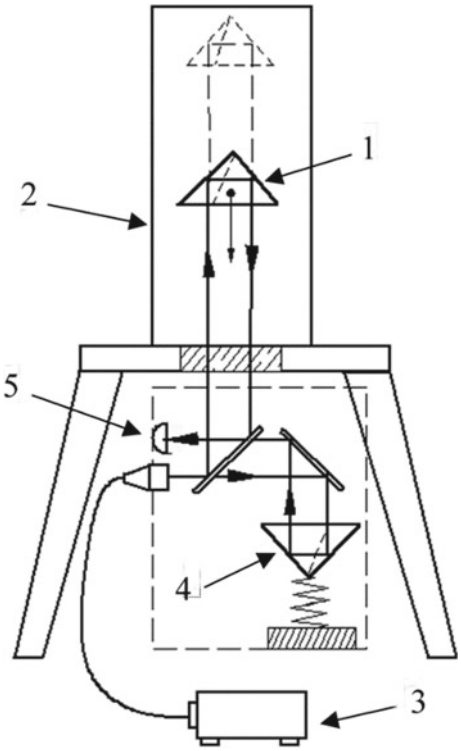

Fig. 1.1 A schematic of a laser-interferometric ABG with a macroscopic test body. *1*—test body with an integrated optical reflector in the measuring arm of the interferometer; *2*—vacuum chamber; *3*—laser; *4*—reflector placed on a vibroprotective (active or passive) suspension in the reference arm of the interferometer; *5*—optical interference signal photoreceiver

- a computer with software for processing the measured data and calculating the measured FFA value with the introduction of necessary instrumental and geophysical corrections;
- additional equipment that ensures ABG functioning.

The test body falls in vacuum chambers to eliminate or reduce air (residual gas) resistance.

In ABGs with an MTB, the laser interferometer measures the displacement of the test body, and the small time interval measuring system measures time intervals.

In ABG designs known, the length of the test body trajectory is from 2 to 50 cm, the time of the test body fall is approximately from 0.02 to 0.32 s.

The vacuum chamber contains a ballistic unit carrying out the entire cycle of the test body motion, including its free motion along a symmetric or asymmetric trajectory and catch of the test body at the end of the trajectory.

In rise-and-fall ABGs, the test body is thrown by a special catapult (for example, see Germak et al. 2002). In almost any design, there is an inevitable effect of mechanical recoil which is the source of undesirable mechanical oscillations of the reference reflector of the laser interferometer, with respect to which the intervals of the path traveled by the test body are measured.

In some free-fall ABGs (for example, in all gravimeters manufactured by Micro-g LaCoste, Inc., USA), in the ballistic unit of the gravimeter, the test body fall is accompanied by a simultaneous motion of the carriage on which the test body rests before the throw and which, having accelerated enough for the test body separation, then moves ahead of the test body during its fall (Niebauer et al. 1994). Such motion of the carriage causes parasitic mechanical excitations.

In the design of the GABL gravimeter of the Institute of Automation and Electrometry of the Siberian Branch of the Russian Academy of Sciences, the test body is held in its initial upper position with an electromagnet and brought to a fall by switching the electromagnet off (Arnautov et al. 1988); there are no mechanical excitations during the test body fall, but the effect of the residual magnetic field remains at the initial segment of the fall path.

In the design of the ABG-VNIIM-1 gravimeter (Vitushkin and Orlov 2011), the test body is held in the initial upper position with a special piezoceramics-based clamp, while there are no mechanical excitations or residual magnetic fields during the free fall of the test body.

The time interval between individual throws in some ABGs with MTB can be quite small: it does not exceed 0.3 s in an eccentric gravimeter (Vitouchkine and Faller 2002).

The equation for the test body motion that does not take into account the vertical gradient of the gravitational field is quite simple:

$$L = L_0 + V_0 T + \frac{gT^2}{2}, \tag{1.1.1}$$

where g is the free-fall acceleration, L is the path interval traveled by the free-falling test body during the time T, L_0 and V_0 are the test body coordinate and speed at the initial moment of time $T = 0$.

If $L_0 = 0$ and $V_0 = 0$, the following measurement equation can be used:

$$g = \frac{2L}{T^2}. \tag{1.1.2}$$

This expression gives simple estimates of the level of measurement uncertainties included in Eq. (1.1.2) path intervals L and time T needed to achieve the relative uncertainty 1×10^{-9} when calculating the absolute value of FFA g. It follows from formula (1.1.2) that the relative uncertainty of path interval measurements should not exceed 1×10^{-9}, and the relative uncertainty in measuring time intervals of the test body fall should not exceed 5×10^{-10}.

These values of uncertainties also define the requirements for the laser radiation wavelength (frequency) uncertainty and for the uncertainty in detecting interference fringes (IF) in the interferometer.

The inhomogeneity of the Earth's gravitational field (the presence of the vertical gradient W_{zz}, i.e., the second derivative of the gravitational potential W in the vertical coordinate z) complicates the equation of motion for a free-falling test body in a gravitational field with a vertical gradient:

$$\ddot{z} = g_{top} + W_{zz} z, \tag{1.1.3}$$

where g_{top} is the FFA at $z = 0$, W_{zz} is the vertical gradient of the gravitational potential W:

$$W_{zz} = \frac{(\partial^2 W)}{\partial z^2}.$$

The approximate solution of Eq. (1.1.3) for $W_{ZZ} \ll 1$ is as follows:

$$z(t) = z_0\left(1 + \frac{t^2}{2}\right) + v_0\left(t + \frac{W_{zz}t^3}{6}\right) + \frac{g_{top}}{2}\left(t^2 + \frac{W_{zz}t^4}{12}\right), \tag{1.1.4}$$

where z_0 and v_0 are the vertical coordinate and speed of the test body at $t = 0$.

In practice, based on Eq. (1.1.4) derived from Eq. (1.1.3), a vertical gradient correction is calculated for the solution of Eq. (1.1.1) when calculating the FFA value measured with an absolute ballistic gravimeter using the least squares method from the "path/time interval" pairs measured during a free fall of the test body.

The vertical gradient is usually measured using a relative gravimeter installed at various heights above the pedestal of the gravimetric site.

The vertical gradient correction is also used in reducing the measured FFA value g_{top} to a specified height above the pedestal. For a more accurate calculation of such

a correction, the FFA vertical distribution is measured with a relative gravimeter and approximated by a second-order polynomial.

The reduction of measurement results of various gravimeters with different heights inherent in their designs, where g_{top} is measured, is necessary; in particular, for the analysis of their measurement results during the comparison of absolute gravimeters.

It should be noted that, when measuring the accelerated fall of a test body with an interferometer, the frequency of IF counting rapidly changes from almost zero to several megahertz during the fall in tenths of a second, which requires high-speed recording of such signals with almost linear frequency modulation.

In ABGs, laser interferometers most commonly use helium–neon frequency-stabilized lasers at a wavelength of 633 nm (red region of the visible spectrum) and, more recently, solid-state lasers at a wavelength of 532 nm (for example, see Orlov and Vitushkin 2010).

Solid-state lasers have the following advantages:

(a) a shorter wavelength (which improves the measurement resolution, since the wavelength sets the displacement measurement scale increment: the smaller the increment (scale division), the greater the resolution);
(b) a higher radiation power (which also increases the resolution when measuring displacements due to an increase in the signal-to-noise ratio of the interference signal);
(c) a lower level of frequency noise, i.e., greater frequency stability at short time intervals (which is important when measuring an interference signal with a rapidly changing frequency).

For example, when measuring the free-fall path of a test body with a length of 10 cm (as in the gravimeter described in Vitushkin and Orlov 2014), the path length measuring uncertainty should not exceed 0.1 nm to provide a relative uncertainty of 10^{-9} when measuring the FFA.

In ABGs with an MTB, various versions of two-beam laser interferometers are commonly used (in particular, see Vitushkin et al. 2012). There is also a known case of using a multibeam interferometer in an ABG (Canuteson and Zumberge 1996).

In two-beam interferometers, the length of one of the arms (referred to as the reference arm) is constant; the length of the other measuring arm changes with the motion of the reflector attached to the falling test body. The test body motion is measured with respect to any element in the optical layout (Vitushkin et al. 2012) which represents the origin of a quasi-inertial coordinate system. Such a reference reflector is usually suspended using a passive (usually a long-period seismometer) or active (Niebauer et al. 1994, 1995) vibration isolation system to reduce undesirable vibrations caused by microseismic vibrations of the base.

Over a relatively short time while the test body is falling (tenths of a second), the IF recording system of a laser interferometer records hundreds of thousands of IFs. For example, in the ABG-VNIIM-1 gravimeter, about 350 thousand IFs are recorded within 0.1 s, each of which corresponds to a test body displacement for half the wavelength $\lambda = 532$ nm of the laser radiation Nd:YVO_4/KTP/I_2 of the laser.

This number of fringes is recorded in groups of scaled fringes (for example, 1024 IFs each) and, together with the recorded time intervals, they are used to calculate the measured FFA value using the least-squares method (LSM). Thus, hundreds of data pairs are used in the calculations with the use of the LSM.

Along with laser-interferometric ABGs with MTBs containing built-in optical reflectors, cold-atom ABGs (Bordé 2002; Peters et al. 2001; Merlet et al. 2009; Gillot et al. 2014) using matter wave interferometry (de Broglie wave interferometry) were developed. The latter are discussed in detail in Sect. 5.3. Cold, i.e. slowed by laser pulses, cesium or rubidium atoms controlled by laser pulses, when absorbing or emitting photons, split or merge while forming equivalents of beam splitters of a classical interferometer, where atomic waves are split or recombine. When propagating in the gravitational field in two arms of an atomic interferometer, atomic waves in one of the arms of the interferometer gain an additional phase shift proportional to the FFA value and the propagation time squared. The interference fringes of such an interferometer can be recorded by measuring the relative population of the states of two recombined atomic beams using induced laser fluorescence.

1.1.2 Sources of Uncertainties and Corrections in Measurements with Absolute Ballistic Gravimeters

When calculating the FFA from measured pairs of path and time intervals, instrumental and geophysical corrections to the measurement results (common to almost all designs of such ABGs) should be introduced in ABGs with an MTB.

Instrumental corrections currently known and common to all types of ABGs include corrections for the following factors:

- deceleration of the test body by residual gases in the vacuum chamber;
- interaction of the falling test body with the gravitational field of the ABG itself;
- interaction of the falling test body with the gradient of the geomagnetic field and the magnetic field of the ion pump (if used in the design);
- effects associated with the finite speed of light;
- diffraction effects during the propagation of a laser beam in the interferometer.

Geophysical corrections are made for the Earth's gravitational tides, the oceanic load and the motion of the Earth's poles.

The following components are taken into account when calculating the total instrumental uncertainty of an ABG:

- uncertainty of the wavelength (frequency) of laser radiation;
- uncertainty of the frequency of the reference rubidium oscillator for the path and time interval measuring system;
- uncertainty due to the choice of the initial and final reference interval of the path from the array of all measured intervals for calculating the FFA using the LSM method;

- uncertainty due to phase delays in electronics;
- uncertainty of the reference height, for which the FFA value is measured;
- uncertainty of the laser beam verticality in the measuring arm of the interferometer;
- uncertainty due to atmospheric pressure variations when determining the correction for the deviation from the nominal value of atmospheric pressure at a gravimetric site;
- uncertainties in the calculation of the above instrumental corrections.

In rise-and-fall ABGs, the influence of such sources of uncertainty as resistance of the residual gas is significantly reduced, and this was used in the initial development of gravimeters when it was impossible to achieve a sufficient degree of vacuum. Later, when ABGs were developed, asymmetric trajectory designs were used, which made it possible to avoid the recoil effect when the test body was thrown up with special catapults.

As examples, we note that the extended (i.e., ensuring a given interval of values with a probability of 95%) total instrumental uncertainty of the ABG-VNIIM-1 gravimeter (Vitushkin and Orlov 2014) and the value of uncertainty reported on the company website for the FG5 gravimeter manufactured by Micro-g LaCoste, Inc., do not exceed 2 μGal. The experimental standard deviation of the measurement result depends on the microseismic conditions at the gravimetric site.

1.1.3 Metrological Assurance of Absolute Gravimeters

ABGs measure the free-fall acceleration. Acceleration is a derivative physical quantity; and an absolute gravimeter should be basically supplied with units of length and time in the respective measurement ranges, which can be done by calibrating the interferometer of the gravimeter with respect to the displacement and the frequency of the laser and the reference frequency oscillator.

In practice, a displacement laser interferometer integrated into an ABG is not calibrated in terms of length unit, like ordinary industrial displacement laser interferometers. Designs of gravimeters with laser interferometers that take measurements in vacuum are not suitable for direct calibration of these interferometers.

The interferometer laser is normally calibrated by frequency (wavelength). However, a unit of length is realized with a laser interferometer rather than with a laser, which is only a source of radiation for the interferometer and generates an infinite traveling electromagnetic wave. Without going into details, it is only worth mentioning that without additional elements (mirrors, photodetectors, etc.), such a wave cannot realize a unit of length in accordance with its definition, i.e. indicate two material points in space between which there is a unit of length or a part of it or two successive positions of a material point as it moves, similar to what, for example, occurs in a gravimeter interferometer that measures the motion of a falling reflector.

As for the calibration of the time interval measurement system, in practice, only the rubidium frequency generator (the reference oscillator for the time interval measurement system) is calibrated by frequency. Such calibration confirms the required level of 5×10^{-10} of the rubidium generator relative frequency uncertainty but not in the entire frequency range of interest. This calibration is normally done at time intervals of tens of minutes, and the question of the metrological characteristics of the measurement system for small (millisecond and microsecond) time intervals for the passage of the above reference path intervals remains open.

Calibration of the laser frequency (wavelength) and the rubidium oscillator frequency is necessary but not sufficient to determine the metrological characteristics of an ABG.

Thus, to determine the metrological characteristics of an ABG when measuring the FFA, it is required to calibrate or verify ABGs using standards in gravimetry as in the case of any other measuring instruments.

ABGs, as well as gravimetric sites and gravimetric networks can be standards in gravimetry. In this case, the FFA values at gravimetric sites and in gravimetric networks should be measured in advance. In some cases, the FFA values at gravimetric sites and in gravimetric networks vary with time as they experience non-tidal changes in the gravitational field.

ABGs, which are, in fact, the measurement standards of the acceleration unit in gravimetry, have the highest metrological characteristics.

Note that a gravimetric site is referred to as the "gravity standard" and an ABG as the "measurement standard in gravimetry" (Vitushkin 2011).

The ABG with the studied metrological characteristics belonging to a National Metrological Institute (NMI) is the officially recognized national primary standard. It is these standards that are involved in the international ABG comparisons organized by the International Committee of Weights and Measures (CIPM) or regional metrological organizations (RMO).

In the Russian Federation, the national primary special standard for the acceleration unit in gravimetry GET190-2011 was created and is used in D. I. Mendeleev All-Russian Research Institute for Metrology (Vitushkin, Orlov 2014).

1.1.4 International Comparisons of Absolute Gravimeters

The first international comparisons of absolute gravimeters were organized following the Recommendation adopted at the XVII General Assembly of the International Union of Geodesy and Geophysics in Canberra (December 1979).

Comparisons of six ABGs built by the International Bureau of Weights and Measures (BIPM), as well as in China, Japan, Russia, and the USA, were organized by the BIPM and the President of Special Research Group 3.40 of the International Association of Geodesy (IAG), associate member of the USSR Academy of Science, Yu. D. Boulanger and conducted in Sèvres (France) in 1980–1981.

Later on, such comparisons were carried out by the BIPM almost every four years. A total of 22 absolute gravimeters were used during the 8th International Comparison of Absolute Gravimeters (ICAG) in 2009.

The organization of ICAGs was improving in the course of time; a technical protocol describing the order of their organization, admission criteria for instruments to participate in comparisons, the procedure for measuring and processing their results, as well as the rules for publishing the results of comparisons were developed and refined. Since 2001, ICAGs have been conducted in accordance with the rules for the organization of comparisons recommended by the international Mutual Recognition Arrangement (MRA) for calibration certificates and measurement results signed by 101 national metrology institutes and organizations responsible for the metrological assurance of any kinds of measurement.

Until 2009, almost all organizations that had ABGs were allowed to participate in the ICAG, and the results of measurements with all gravimeters were used in calculating the result of comparisons (the average FFA values obtained with all gravimeters at gravimetric sites where measurements were taken, the uncertainties of those average values, as well as the degree of equivalence of the gravimeters used which was measured by their deviations from the average values obtained by all gravimeters).

More than 90% of ABGs used in the world are commercial; all of them are produced by one company in the USA. These gravimeters do not have any calibration certificates; therefore, the organizations that had them sought to take part in the ICAG, as well as in comparisons organized in the underground laboratory in Walferdange (Luxembourg) (Jiang et al. 2012) in order to determine metrological characteristics of their instruments.

Due to the increase in the number of ABGs in the world, it will be almost impossible to conduct their simultaneous comparisons in one laboratory in the future; therefore, it is necessary to use a conventional practice in metrology: to recognize national standards and arrange calibrations of ABGs. It should be noted that such a system in the field of absolute gravimetry has not been organized until recently.

In 2009, ICAGs were organized as key comparisons according to the MRA rules (see CIPM MRA-D-05 "Measurement Comparisons in CIPM MRA" at http://www.bipm.org/en/cipm-mra/cipm-mra-documents/), according to which only gravimeters belonging to the NMI are allowed to be compared. As an exception, comparisons of ABGs from other organizations were carried out as pilot studies in parallel with the key comparisons in the BIPM. Meanwhile, only the results of 11 NMI gravimeters were used when calculating the official results of comparisons. These results were published in the official key comparison database on the BIPM website (http://www.kcdb.bipm.org).

The results of pilot studies can be published in scientific journals, but they cannot serve as grounds for issuing calibration certificates. All the results of the ICAG 2009 were published in Jiang et al. (2012).

The increasing IAG requirements for the reliability of absolute measurements of the gravitational field led to the development and adoption of the "Strategy of the Consultative Committee for Mass and Related Quantities and IAG in Metrology in

Absolute Gravimetry" (published in IAG Proceedings of the 2011–2015 (Travaux of the IAG 2011–2015)). The purpose of this document is to draw the attention of geodetic and geophysical communities to the need to develop a system of metrological assurance for absolute gravimeters according to the classical hierarchical procedure with primary standards, calibrations and verifications of ABGs. Various ABG calibration procedures are considered: direct comparison with the primary ABG standard or by measuring the FFA using the gravimeter being calibrated at a gravimetric site where the FFA value was previously measured using the ABG standard, and comparing the measurements using the gravimeter being calibrated with the result obtained with the ABG standard. The highest reliability of this calibration method for the previously measured FFA value can be ensured by continuous monitoring of the FFA time variations using an additional gravitational field measurement tool—a relative superconducting gravimeter (SG) (see an example of using a cryogenic gravimeter during ABG comparisons in Francis et al. 2014). Relative SGs allow for continuous measurements of variations in the gravitational field with a resolution of one hundredth of a microgal over many months and years. SGs are used to measure time variations of the FFA.

1.1.5 Comparisons of Absolute Gravimeters: The Results

A clear understanding of metrological characteristics of modern ABGs is provided by the results of key comparisons organized by the CIPM and key regional comparisons organized by RMOs (EURAMET—Europe RMO, NORAMET—North America RMO, APMP—Asia–Pacific RMO, etc.). The results of the 2009 key ABG comparisons (BIPM) and the 2013 key comparisons (Walferdange), as well as the results of the 2013 key European comparisons (Walferdange) will be presented here.

It should be noted that after ICAG-2009, the BIPM decided to stop the organization of comparisons of absolute gravimeters in the bureau itself because the procedure for organizing comparisons had been well-elaborated and they could now be organized by other NMIs. In 2013, the key ABG comparisons organized by CIPM along with ABG pilot studies took place in the underground laboratory in Walferdange. Comparisons were also held in China in the laboratory of the National Metrology Institute in the Changping campus in 2017.

Figure 1.2 presents the results of key comparisons of CCM.G-K1 ABGs (Jiang et al. 2012; Arias et al. 2012). Note that the reports of all key comparisons are available online in the key comparison database on the BIPM website.

Figure 1.3 shows the results of the key comparisons of CCM.G-K2 ABGs (Francis et al. 2015). Figure 1.4 shows the results of the key European comparisons of ABGs conducted under the authority of the regional metrological organization EURAMET (Francis et al. 2014).

In all the figures, the uncertainty bars represent the extended total uncertainty of each result.

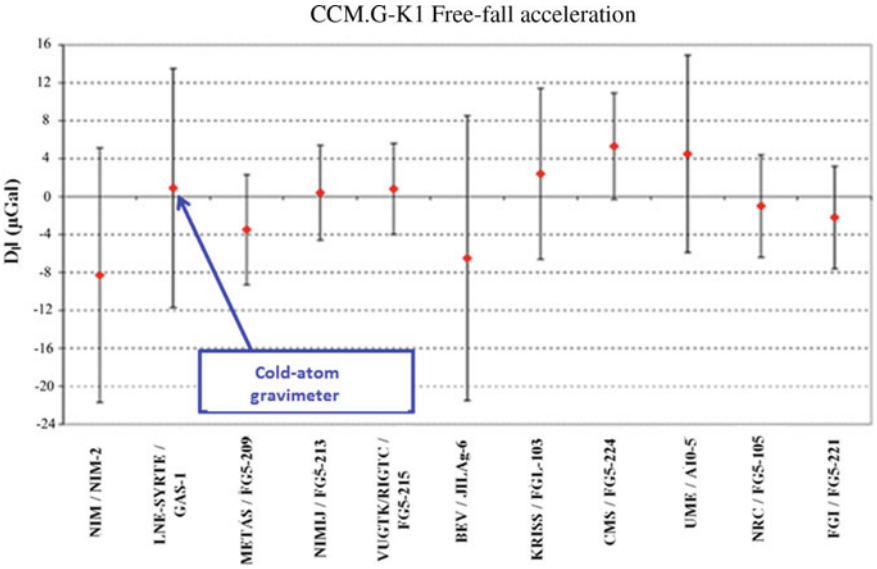

Fig. 1.2 The results of the key comparisons of CCM.G-K1 absolute gravimeters (2009, BIPM, Sèvres, France). The vertical axis shows the deviations from the key comparison reference value (in microgals) for the result of each gravimeter; the horizontal axis shows the type and number of the gravimeter and the organization to which it belongs

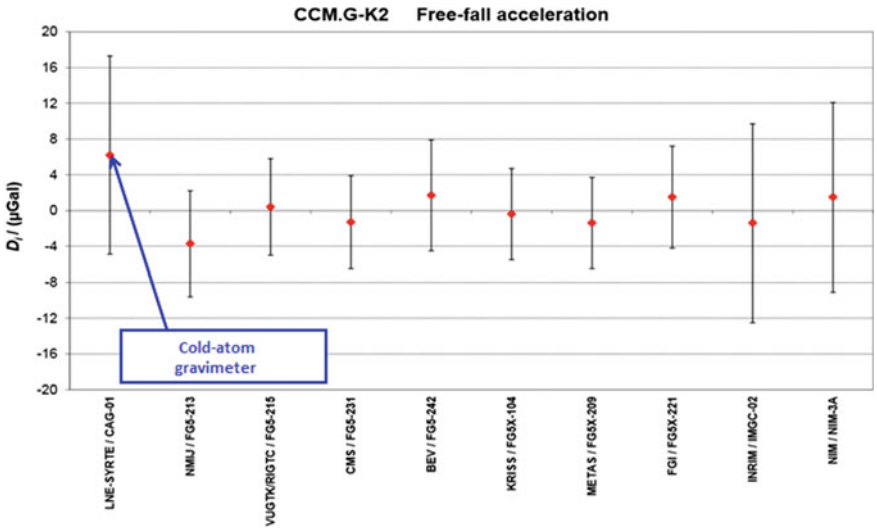

Fig. 1.3 The results of the key comparisons of CCM.G-K2 absolute gravimeters (2013, Walferdange, Luxembourg). The vertical axis shows the deviations from the key comparison reference value in microgals for the result of each gravimeter; the horizontal axis shows the type and number of the gravimeter and the organization to which it belongs

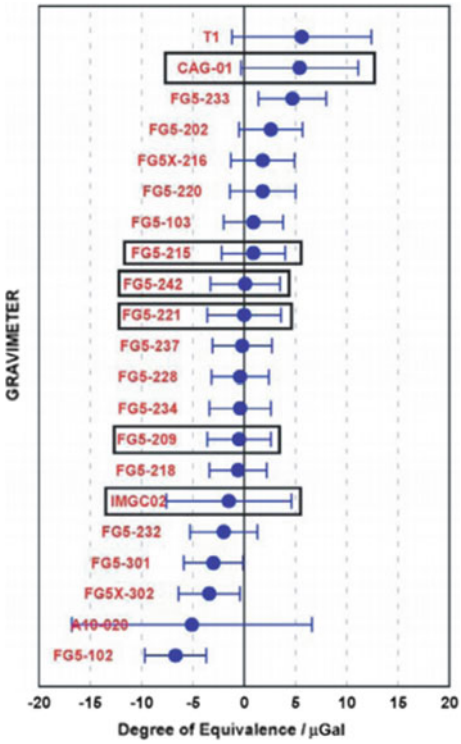

Fig. 1.4 The results of the regional European comparisons of ECAG-2011 absolute gravimeters (2011, Walferdange, Luxembourg). The vertical axis shows the type and number of the gravimeter; the horizontal axis shows the degree of equivalence of the results of each gravimeter in microgals with the reference value of comparisons. The names of the NMI gravimeters used in the key comparisons are shown in frames. The remaining gravimeters were used in pilot studies as part of the general comparison campaign

As can be seen from the figures, the comparisons were carried out mainly for FG5 and A10 gravimeters, both manufactured by Micro-g LaCoste, Inc. There were only three gravimeters from other organizations: the IMGC gravimeter (Italy), the CAG-1 cold atom gravimeter (France), and the T1 gravimeter (China).

Note that the uncertainty of FFA measurements with the use of a cold-atom gravimeter is currently slightly greater than the uncertainty of the best laser-interferometric ABGs with MTB. The A10 gravimeter is designed for field measurements and has a greater uncertainty than the FG5-type gravimeters.

1.1.6 Practical Applications of Absolute Free-Fall Acceleration Measurements

Currently, at least two hundred transportable ABGs are used in the world. Most of them were manufactured by Micro-g LaCoste, Inc.

ABG allows measuring the FFA in any place with no reference to any sites of gravimetric networks. Of course, the accuracy of measurements depends on the level

of microseismic conditions at the gravimetric site which determines the random component of the uncertainty.

The emergence of a significant number of such ABGs allowed changing the measuring strategy of gravimetric networks and their use (for example, see Boedecker 2002).

Transportable ABGs made it possible not only to measure the FFA at different gravimetric sites when creating gravimetric networks, but also take repeated measurements to monitor temporal variations of the gravitational field.

The combination of an ABG and an SG allows for almost continuous monitoring of the gravitational field. Starting in 1997, about 30 gravimetric sites on Earth, including the Antarctic Syowa station, conducted monitoring of the gravitational field variations using an ABG and an SG in the framework of the IAG International Global Geodynamic Project. This project has currently been reformed into the permanent IAG IGETS service and continues developing.

Transportable ABGs are used, for example, in hydrogeology for prospecting and monitoring of water reserves, as well as in engineering geology.

Studies are conducted on the possibility of using laser-interferometric ABGs and cold-atom ABGs on moving bases in airborne and marine gravimetry (Baumann et al. 2012; Sokolov et al. 2017).

The concept of joint use of absolute and relative gravimeters installed on a gyrostabilized platform for marine gravimetry was proposed in the early 2000s. It is not necessary to conduct continuous FFA measurement using ABGs. ABGs can be used for periodic calibration of relative gravimeters when the vessel stops at a pier or on a calm sea. It should be noted that an eccentric-type gravimeter with a short free-fall path of the test body of about 2 cm allowing for 200 drops per minute can be successfully used in airborne and marine gravimetry (Vitouchkine and Faller 2002).

1.1.7 Conclusions

Ground-based absolute gravimetry is finding increasing use for national and international projects in modern geodesy such as the Global Geodetic Observing System of the International Association of Geodesy.

In international comparisons of absolute gravimeters, the uncertainties in measuring absolute FFA values may not exceed 1 μGal at gravimetric sites where many ABGs are compared and a great number of measurement series are carried out (for example, more than 60 12-h series of measurements at 5 gravimetric stations of a gravimetric site in comparisons in BIPM in 2009 (Jiang et al. 2012)). The FFA values and their uncertainties obtained in such comparisons are most reliable. This circumstance, as well as the increasing number of absolute gravimeters, the development of their metrological assurance system, and the distribution of comparisons to other continents (North America, Asia) provided the basis for creating a new global system of absolute gravimetric sites outlined, in particular, in Crossley et al. (2013).

Key comparisons of gravimeters were carried out in Europe; regional comparisons of gravimeters were carried out in North America and China. Gravimetric sites where comparisons are made will be used as the basis for a new global system.

In 2015, the International Association of Geodesy held the 26th General Assembly of the International Union of Geodesy and Geophysics in Prague, where they adopted Resolution 2 "For the Establishment of a Global Absolute Gravity Reference System", specifying the FFA value measurement uncertainty not higher than 10 μGal for the reference sites of the system, i.e., 10 times less than in the IGSN-1971 system.

The development of absolute gravimetry in the Russian Federation requires the development of new ABGs, including field gravimeters and ABGs adapted to measurements on moving bases.

Both types of absolute gravimeters—MTB laser interferometer gravimeters and cold-atom gravimeters—will certainly find their applications; besides, they can be improved to reduce their overall dimensions, increase their reliability and reduce their measurement uncertainty.

1.2 Chekan-Series Relative Gravimeters

For more than 50 years, Concern CSRI Elektropribor has been working on creation of gravimetric systems for measuring gravity from moving carriers. This work started in 1967 with the creation of GAL-M, a gravimeter with a photo-recording system, at the Schmidt Institute of Physics of the Earth under supervision of E.I. Popov. At the same time, the Cheta gyro platform was developed at CSRI Elektropribor for stabilization of this gravimeter on surface ships (Popov 1959). On the basis of these developments, the MGF gravimeter was created and adopted for the Navy supply by order of the Navigation and Oceanography Department of the Russian Ministry of Defense. That was the first Russian gravimetric system intended for marine gravity surveys in the open ocean in 1970–1980.

Cheta-AGG, the first automated marine gravimetric system (chief designer A.D. Bereza) with a specialized digital computer, was created by order of the Navy in 1982 and was produced in series (Zheleznyak and Popov 1982). This system was installed on more than ten research vessels. For many years, it was the main means of route and areal gravity surveys and was used until the beginning of the twenty-first century both on Navy ships and on civilian vessels. Under the World Gravity Survey Program, the Cheta-AGG system was used to take a large amount of measurements in the Atlantic, Indian, and Pacific Oceans, the Black and Barents Seas (Zheleznyak et al. 1983).

The development of the Skalkochnik, the third-generation system (chief designer L.P. Nesenyuk (Pamyati professora L.P. Nesenyuka 2010)), was aimed at improving the performance characteristics through the use of the latest computing aids of the day. It was the first to use a personal computer both for data acquisition and office processing of marine survey results. In 1994, the system passed the Navy tests and was put into operation. Unfortunately, the difficult economic situation in the country at the end of the twentieth century did not allow for full-scale production of the

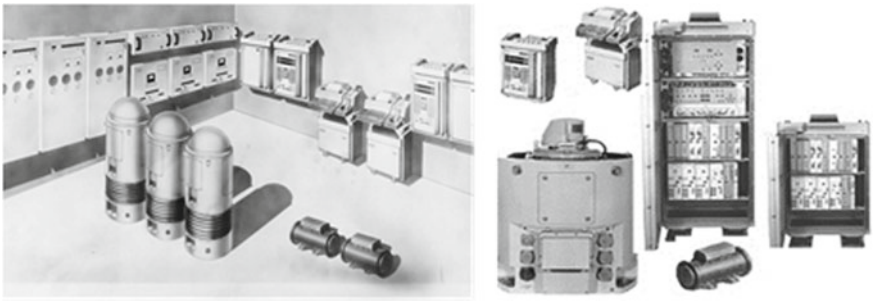

Fig. 1.5 General view of the second- and third-generation systems

Skalochnik system. Only a prototype model was made which was upgraded in 2001 and used by the Navy hydrographic service until 2006 (Nesenyuk and Elinson 1995; Bikeeva et al. 2007). A general view of the Cheta-AGG and Skalochnik systems is shown in Fig. 1.5.

The work on the construction of the fourth-generation system began in the late 1990s, when the Chekan-A prototype system was made in 1998 and its marine tests were carried out in 1999 combined with a commercial marine geophysical survey conducted by the Norwegian company NOPEC (Sokolov et al. 2000). The success in the accomplishment of this work allowed CSRI Elektropribor to fulfill the research on design and development of a mobile gravimeter (chief designer L.S.Elinson). As a result, the fourth-generation Chekan-AM system was developed in 2001 (Sokolov 2003).

Today, the Chekan-AM mobile gravimeter is one of the main instruments used to measure gravity from sea vessels and aircraft (Kovrizhnykh and Shagirov 2013; Atakov et al. 2010; Lygin 2010; Forsberg et al. 2013; Barthelmes et al. 2013; Peshekhonov et al. 2020). More than 50 gravimeters have been manufactured at CSRI Elektropribor and delivered to Russian and international organizations. Table 1.1 shows how the global geophysical equipment market has been developing: from marine surveys abroad to airborne gravity surveys in Russia.

The geography of the gravity surveys carried out with the Chekan-AM mobile gravimeter shown in Fig. 1.6 covers the waters of all oceans and shelf zones in all continents. Chekan-AM has been used in geophysical surveys from the Antarctic to the North Pole (Krasnov et al. 2014a).

In 2013, a new system Shelf-E was developed (chief designer A.V. Sokolov) on the basis of the Chekan-AM mobile gravimeter (Krasnov et al. 2014b). The system has improved accuracy and performance characteristics. Its serial production started in 2015, so that these systems are supposed to replace Chekan-AM mobile gravimeters in the near future. This chapter is devoted to the description of the principle of operation, design features, and technical characteristics of the Chekan-AM and Shelf-E systems.

Table 1.1 Development of the global geophysical equipment market

Country	Years in operation
Marine gravity surveys	
Norway	1999 up to the present
Great Britain	2003–2012
Russia	2005 up to the present
China	2007 up to the present
USA	2008 up to the present
Kazakhstan	2010–2011
Airborne gravity surveys	
Germany	2007 up to the present
Norway	2007–2011
Russia	2007 up to the present

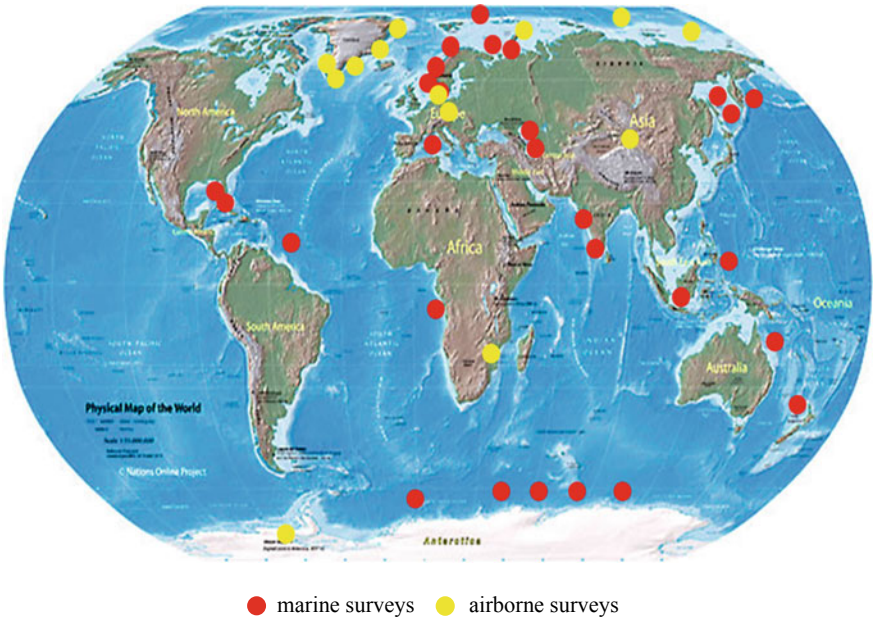

Fig. 1.6 Geography of the gravity surveys carried out with the Chekan-AM mobile gravimeter

1.2.1 Gravimeter Parts

The main distinction of the Chekan-AM mobile gravimeter from the systems of previous generations is its higher accuracy and performance characteristics along with a multifold decrease in its weight and overall dimensions (Blazhnov et al. 2002). The development of electronic components made it possible to combine the

Fig. 1.7 Chekan-AM gravimeter

gravimeter sensing element (GSE), a biaxial gyro platform, and a control device based on microcontrollers in a single device.

The structure of the Chekan-AM mobile gravimeter is shown in Fig. 1.7. The basis of the system is a gravity sensor (GS) with a double quartz torsion-type elastic system installed in a two-axis gyro platform (GP) designed to keep its sensitive axis in the vertical direction on a moving carrier.

A thermostabilization device (TD) is placed in the upper part of the GP housing in order to maintain a constant temperature inside it. The TD is controlled by the UMT unit external to it.

The delivery set of the Chekan-AM gravimeter also includes an industrial-grade personal computer with real-time data acquisition and primary processing software and programs for diagnosing the parts of the system. The system is powered by a voltage of 27 VDC generated by AC/DC converter from an onboard mains of 220 V/50 Hz via a SMART-UPS uninterruptible power supply.

Figure 1.8 shows a block diagram of a mobile gravimeter for marine and airborne versions of the system. The main difference between these versions is real-time software since continuous correction of GP is necessary when taking measurements from aircraft. GP correction is carried out with the use of external information on the speed and position of the carrier; therefore, when conducting airborne gravity surveys, it is necessary to ensure data reception from a GNSS receiver which is not included in the system.

Another feature of airborne gravity surveys is the absence of a standard 220 V/50 Hz mains onboard aircraft. Therefore, for the airborne version of the

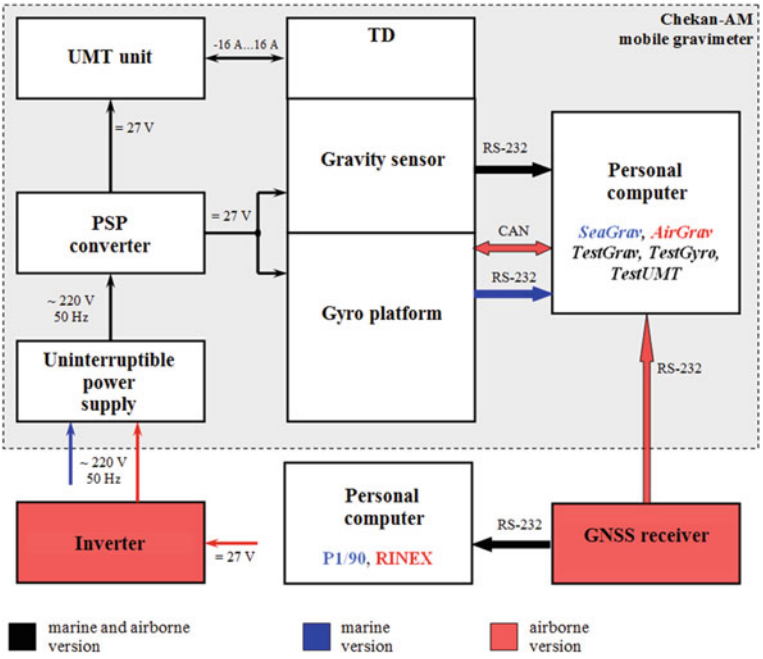

Fig. 1.8 Block diagram of the Chekan-AM gravimeter

system, an additional inverter is required, which is not included in the gravimeter instrumentation.

Navigation data recorded by the GNSS equipment is used for the office processing of marine and airborne gravity measurements. For this purpose, the navigation and gravimetric data are synchronized on a time scale.

The structure of the Shelf-E gravimeter is even more simplified: there are no secondary power supply and no GP thermal regulation system. It has just a gyro platform with a gravity sensor and a laptop. The system is connected with one cable; data can be transmitted via a wireless communication channel based on Wi-Fi technology (Peshekhonov et al. 2015).

1.2.2 Gravimeter Sensing Element

The gravimeter sensing elements used in the CSRI Elektropribor systems were created on the basis of a double quartz elastic system of the gravimeter (GES). Its principles of construction and first designs were developed by the Schmidt Institute of Physics of the Earth of the Russian Academy of Sciences (Zheleznyak and Popov 1984). Later on, the GES design and manufacturing technology were improved jointly by both enterprises and in parallel with the construction of new gravimetric

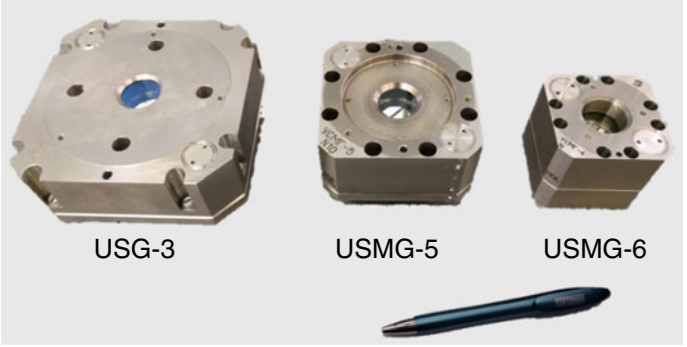

Fig. 1.9 Gravimeter elastic systems

systems. Figure 1.9 shows the GESes installed in the third- and fourth-generation systems: USG-3 (Skalnochnik), USMG-5 (Chekan-AM), and USMG-6 (Shelf-E).

Structurally, the gravimeter elastic system consists of two torsion systems made of very-high-purity quartz glass contained in a common housing. The torsion systems are turned 180° in a horizontal plane relative to each other. The housing of the elastic system is filled with polymethylsiloxane fluid to provide its damping, thermal compensation, and pressure isolation. As a material, quartz has a number of advantages: it is manufacturable; under deformation, it follows the Hooke law until it fractures; and it has a positive thermoelastic coefficient, which allows ensuring thermal compensation due to the use of simple construction.

The elastic systems of the Chekan-AM and Shelf-E gravimeters are designed as all-welded structures. They have no adjusting elements, owing to which its reliability is significantly increased. The advanced technology for fabrication of elastic systems provides a high degree of quartz system identity both in sensitivity and in damping. Nonidentity of the two systems does not exceed 0.2%, which almost completely eliminates the error caused by the cross-coupling effect, which is due to the mutual influence of vertical and horizontal accelerations and is less than 0.2 mGal for a double system when rolling-induced accelerations are up to 1 m/s^2. The elimination of the cross-coupling effect is an important advantage of the GES as compared with other types of gravimeter torsion sensing elements (Panteleev 1983).

Throughout these years, it has been possible to make the elastic system completely sealed, reduce its overall dimensions by several times, simplify the manufacturing technology, and start its manufacturing at CSRI Elektropribor (Sokolov et al. 2021).

GSE principle of operation is shown in Fig. 1.10. The output value of the elastic system is the angle of rotation ϕ of the pendulum lever which changes by the magnitude of the torsional angle $\Delta\phi$ in the presence of gravity increment δg in accordance with the following expression:

$$\Delta\phi = k_1 \cdot \delta g, \tag{1.2.1}$$

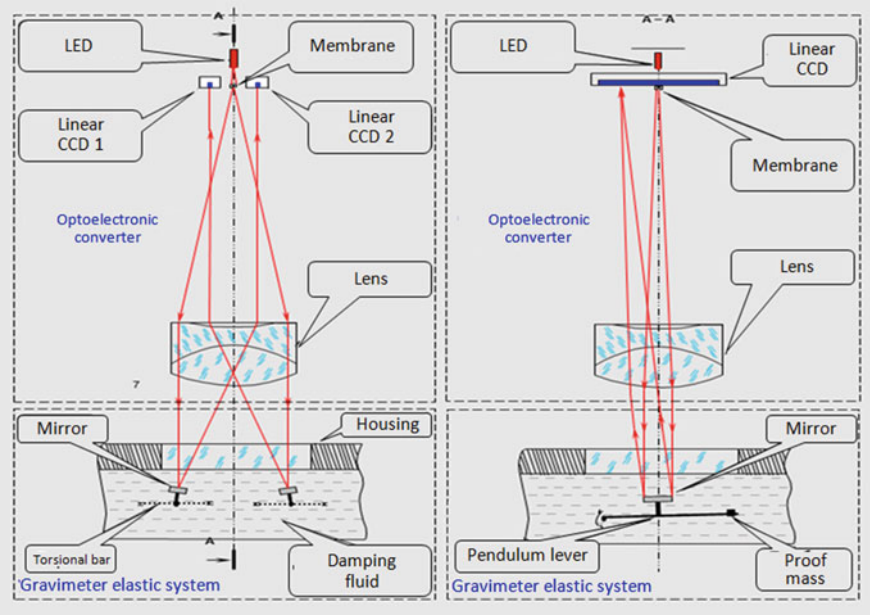

Fig. 1.10 GSE principle of operation

where k_1 is a coefficient defining sensitivity of the elastic system.

To measure the angle of rotation of the pendulums, the latter have mirrors welded to them. Their planes are parallel to the axes of the pendulums and turned at a small angle in the opposite direction. Protective glass with two pairs of optical wedges on it is installed in the upper part of the housing. An optoelectronic converter (OEC) is located above the GES housing. It includes a light source, an autocollimation mark placed in the focal plane of the lens, and two light receivers whose function is performed by linear-type charge-coupled devices (CCD) (Bronstein et al. 2000).

Structurally, the CCDs are separated by a distance corresponding to the angle of rotation of the pendulum mirrors in the direction perpendicular to the scanning. The light source provided by a pulsed LED with the maximum spectral brightness at a wavelength of $\lambda = 626\ \mu$m is placed on the optical axis of the lens between the CCD arrays.

Using the OEC, the pendulum angle of rotation is converted into a linear displacement of the luminous mark along the light-sensitive area of the CCD array. The CCD arrays are directed along the displacement of the slot autocollimation image, and their housings are turned 180° relative to each other. The change in the ΔL position of autocollimation images is proportional to the change in the torsional angle according to the formula:

$$\Delta L = 2nf\Delta\phi, \tag{1.2.2}$$

where n is the refraction index of the damping fluid; f is the focal length of the lens.

The signals from CCD arrays are processed using a video signal to code converter, on which they are directly mounted. The control inputs of both CCDs are connected to a single control signal shaper connected via an optical coupler with an external sync pulse receiver. The signal shaper is also connected to a control signal frequency synthesizer which is connected to a frequency reference oscillator.

The current position of the autocollimation image is calculated based on the energy center using programmable logic devices. Readings m_1, m_2 representing the numerical equivalent of the angle of rotation of the GES pendulum are transmitted via a serial interface to a personal computer with a frequency of 10 Hz (Sokolov 2004).

To maintain a constant temperature, the GES is installed in a thermostat. The temperature inside the thermostat is stabilized by controlling four pairs of thermoelectric converters mounted on the side walls of the thermostat housing made of an aluminum alloy with high thermal conductivity.

Thermoelectric converters are based on the Peltier effect, and the temperature point can be adjusted in the range from +30 to +35 °C. The output power of the thermostat control board is 20 W, which makes it possible to stabilize the GES temperature when the ambient temperature changes relative to the specified temperature point in the range of ±15 °C with an error of 0.01 °C in the steady state. Despite its high accuracy, the GSE thermal regulation system of the Chekan-AM gravimeter has two disadvantages such as a high temperature of thermostabilization and a considerable transient process when the ambient temperature changes.

The main research on modernization of the gravity sensor for the Shelf-E system was aimed at reducing its instrumental error (Krasnov et al. 2014c; Sokolov et al. 2008). This required the development of a new GES and led to a substantial redesign of the gravity sensor (Fig. 1.11). The overall dimensions of the new GES were made 1.5 times smaller than those of the Chekan-AM gravimeter. The dimensions of the quartz frames, torsional bars, pendulums, and other elements of the quartz system were significantly reduced. To extend the range of disturbing accelerations, the polymethylsilixane fluid with a viscosity of 65,000 cPs, which is more than 3 times higher than that of the fluid in the sensing element of the Chekan-AM gravimeter was used to damp the pendulum motion in the new elastic system.

The information about the angular position of the GES pendulums is also obtained using the OEC, but the new OEC uses a specialized 5-megapixel black and white CMOS camera as a photoreceiver. To reduce the size of the gravity sensor, the focal length of the new optoelectronic converter was made half that of the Chekan-AM gravimeter. This did not lead to deterioration in the autocollimator resolution because the pixel size of the CMOS sensor used is only one-third that of the previously used CCD array (Berezin et al. 2004).

A fundamentally important design feature of the new gravity sensor in comparison with all previous versions is that the GES with the OEC are placed in a single thermostat. This made it possible to significantly reduce the effect of changes in the ambient temperature on the gravimeter readings. Another important advantage of the new thermostat is a substantial reduction of the stabilization temperature

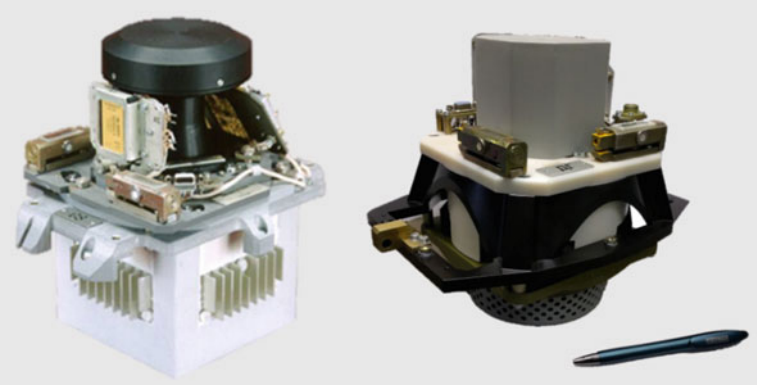

Fig. 1.11 General view of Chekan-AM and Shelf-E gravity sensors

of the sensing element from +35 to +15 °C. As a result, the drift of the Shelf-E gravimeter was reduced several times below that of the Chekan-AM gravimeter. Also, for the first time, the new elastic system and optoelectronic converter are fixed rigidly together without any additional adjustment elements, which made the gravity sensor assembly and adjustment much simpler and increased long-term stability of the gravimeter sensitive axis.

1.2.3 Biaxial Gyro Platform of the Gravimeter

According to its principle of operation, the gyro platform is a biaxial gyrostabilizer with accelerometric correction of the gyroscope rotor positions (Chelpanov et al. 1978). The GP operation is explained by the schematic presented in Fig. 1.12, which shows a biaxial gimbal suspension consisting of outer and inner rings. The orientation of the axes of the gimbal suspension on a vehicle is set in such a way that rolling of the vehicle (θ_K) is compensated for by the outer ring axis, and its pitching (ψ) is compensated for by the inner ring axis. The gravity sensor is installed on the inner ring of the GP together with the sensing elements of the stabilization system: two floated one-degree-of-freedom gyroscopes, two AK10/4 accelerometers, and an azimuth fiber optic gyroscope (FOG).

The sensitive axis of the gravity sensor is kept in the vertical direction using a gearless servo drive and an accelerometer correction system of the gyroscopes. The gearless servo drive on each axis is made on the basis of MK-BSS single-channel microcontrollers that control the position of the outer and inner rings, compensating for the mismatch between the gyro pick-off and its housing.

The accelerometer correction system in the MK-FG microcontrollers is designed to bring the gyroscope precession axes to the vertical. The sensors of the correction system are accelerometers whose sensitive axes are parallel to the axes of the

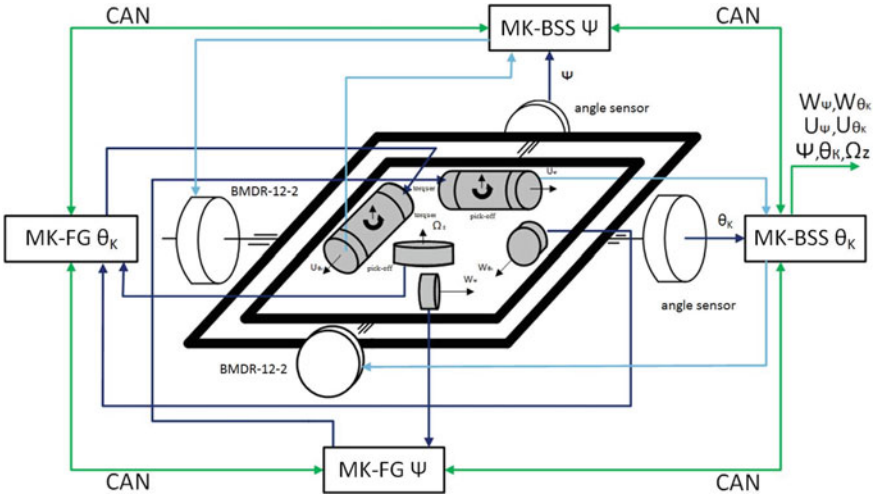

Fig. 1.12 Schematic of the gyro platform

gimbal suspension. Owing to this arrangement, each accelerometer corrects the position of the gyroscope along one of the stabilization axes. During airborne gravity surveys, satellite navigation data are additionally used in the accelerometer correction system, which significantly reduces stabilization errors during the aircraft maneuvers (Krasnov and Sokolov 2009).

To ensure the GP start-up and operation on a moving base, it has different operation modes: electric caging, rough and precision stabilization. In the electric caging mode, the position of the axes of the gimbal rings is matched with the position of the GP housing. In this mode, the servo drive is operated by signals from angle sensors located along the suspension axes.

In the rough stabilization mode, the gimbal rings are stabilized in the horizon plane by the signals coming directly from the accelerometers. This mode is necessary for the gyro spin-up.

After the gyro spin-up, the GP switches to the precision stabilization mode, in which the gyro pick-offs become sensing elements of the servo drive, and the positions of their rotors are controlled by the accelerometer correction system. The ring caging is carried out using a retractable mechanical stopper, and the start and stop of the GP using two buttons mounted on the GP housing which also contains LED indicators that show the current operation mode of the GP. The weight of the GP with a gravity sensor and the thermostabilization device does not exceed 67 kg, and the overall dimensions are Ø 430 × 638 mm. The principle of the GP operation and its design features do not require any additional adjustment operations during commissioning. Owing to these features, the gravimeter can be installed onboard the carrier by one operator.

In the course of the Shelf-E gravimeter design, the GP construction underwent significant changes. All its sensing elements, as well as the MK-FG microcontrollers,

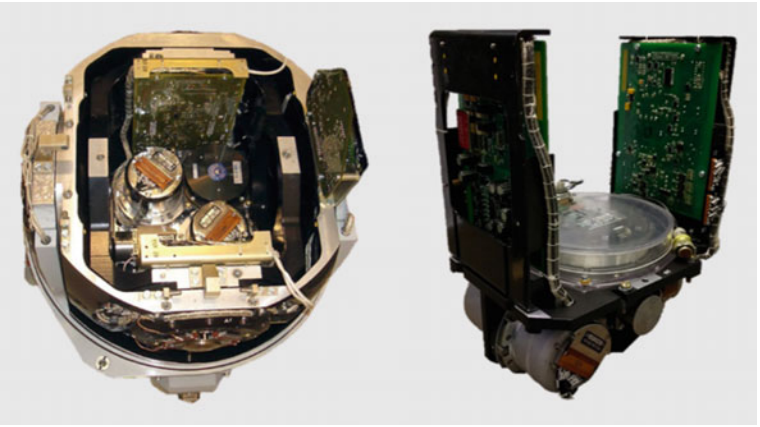

Fig. 1.13 General view of the gyro platform and the gyro unit

are arranged on a single bracket (Fig. 1.13). The gyro unit is easy to remove and install on the GP inner ring.

The gearless servo drive microcontrollers are put into the GP base. This has increased the possible pitch angle of the inner ring by a factor of 1.5 and, thus, removed the restriction on the value of the aircraft pitch angle at takeoff. The advanced design of the gravity sensor has made it possible to omit the GP thermal regulation system, which has reduced the gravimeter total power consumption by three times as compared with the Chekan-AM gravimeter.

An MK-BPR microcontroller is contained in the GP base. It integrates the data from the gravity sensor, its thermal regulation system, and the gyro platform into a single information flow. The data from the MK-BPR microcontroller can be transmitted to the computer either via the RS-232 serial interface or via the Wi-Fi channel.

1.2.4 Mathematical Model of the Gravimeter Sensing Element

The GES principle of operation is explained in the diagram shown in Fig. 1.14. The GES torsional bars are pretwisted in such a way that the pendulum is in a position close to horizontal. In the case of changes in gravity and under the action of inertial accelerations, the pendulum deviates from the horizon and forms the angle $\Delta\phi$.

The sensitive axis of the elastic system described is a straight line which is perpendicular to the pendulum axis and passes through the center of mass of the sensing element. Thus, in the case of changes in gravity and under the action of inertial accelerations, the sensitive axis changes its direction, even if the position of the instrument housing remains unchanged. This is a fundamental difference between a torsional

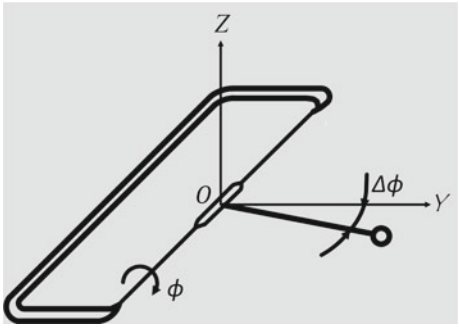

Fig. 1.14 Torsional-type elastic system: principle of operation

system and a linear one. And, as was shown in Eq. (1.2.1), the increment of the torsional angle $\Delta\phi$ corresponds to the increment of gravity δg. In view of the above, the differential equation of motion for the torsional-type GES can be represented as follows (Zheleznyak and Popov 1984):

$$k(T\Delta\phi' + \Delta\phi) = \Delta g - Z'' - (g - Z'')(\alpha^2 + \beta^2 + \Delta\phi^2 + 2\beta\Delta\phi)/2 + X''\alpha + Y''(\beta + \Delta\phi), \tag{1.2.3}$$

where X'', Y'', Z'' are inertial accelerations acting on the gravimeter; α, β are GSE stabilization errors.

In the static state, when there is no inertial acceleration and the GSE is in the horizon, Eq. (1.2.3) has the following form:

$$\delta g = \Delta\phi(k + g \cdot \Delta\phi/2), \tag{1.2.4}$$

where g is the value of gravity.

From expression (1.2.4), it follows that to convert the angle of rotation of the pendulum into readings, it is necessary to use the calibration characteristic which is a function of readings rather than a constant coefficient. In accordance with (1.2.4), there is a gravity increment from the point where the pendulum is in the horizon in the instrument readings. For a torsional-type elastic system during rolling, in addition to the errors due to the tilts of the base discussed above, there are additional components of measurement errors:

$$\varepsilon_{\delta g} = g\beta\Delta\tilde{\phi} + Y''\Delta\tilde{\phi}. \tag{1.2.5}$$

The values of β and $\Delta\tilde{\phi}$ are variable functions of the horizontal and vertical accelerations, respectively. At a certain ratio of their phases, constant errors may appear in the gravimeter readings. This error, which can reach the first tens of milligals, is known as the cross-coupling effect. A double elastic system consisting of two identical systems turned in a horizontal plane at 180° relative to each other is used

to reduce it. In this case, the total effect of disturbing accelerations on the double elastic system can be written as:

$$\varepsilon_{\delta g} = g\beta\left(\Delta\tilde{\phi}_1 - \Delta\tilde{\phi}_2\right) + Y''\left(\Delta\tilde{\phi}_1 - \Delta\tilde{\phi}_2\right), \tag{1.2.6}$$

where $\Delta\tilde{\phi}_1$, $\Delta\tilde{\phi}_2$ are the variable components of the change of the torsional angle of the 1st and 2nd GES pendulums, respectively.

As can be seen from expression (1.2.6), for a double elastic system, the error decreases to a difference effect and is defined by the identity of the two systems included in the double system. For modern systems, their difference in sensitivity does not exceed 0.1%, and in terms of response time, 1.5%, which makes it possible to almost completely eliminate the cross-coupling effect on the double quartz elastic system.

Taking into account the fact that the GSE output signal is the readings formed by two CCD photoreceivers in accordance with expression (1.2.2), the calibration characteristic of the GSE to be determined is a quadratic function of the OEC readings:

$$\delta g = b(m - m_0) + a(m - m_0)^2, \tag{1.2.7}$$

where b, a are the linear and quadratic coefficients of the gravimeter calibration characteristic, m_0 is the reading of the CCD photoreceiver at which the coefficients b, a were determined.

Due to damping fluid, the GSE model contains a first-order aperiodic link which has smoothing properties. Amplitude and phase distortions of the signal to be measured can be excluded by using a recovery filter of the following structure (Blazhnov et al. 1994):

$$W(p) = T_g p + 1, \tag{1.2.8}$$

where T_g is the gravimeter response time, p is the Laplace operator.

Due to the creep of the quartz glass elastic element, the gravimeter readings change with time. Therefore, the GSE model also includes the linear element which describes the quartz GES drift in accordance with the formula:

$$\Delta g_C = C(t - T_0), \tag{1.2.9}$$

where C is the drift value, t is the current time, T_0 is the time of reference measurements.

The drift value is determined from the results of reference measurements and can be refined during the office processing upon completion of the survey.

1.2.5 Algorithms for Gyro Platform Correction

Figure 1.15 is a block diagram of one of the two identical channels of gyro platform accelerometric correction (Krasnov 2007). Control is formed by the integrated correction circuit that implements a short-period gyro vertical based on accelerometer signals. Besides, external information from the GNSS receiver is additionally used in order to eliminate stabilization errors caused by aircraft maneuvering.

The following symbols are used in Fig. 1.15: FT1, FT 2 are frame transformers; K is the heading; R is the average radius of the Earth; $\Omega\cos\varphi$ is the horizontal component of the Earth's angular rate; g is gravity; w is horizontal acceleration; V_E is the horizontal speed produced by the inertial method; V_E^{GNSS} is the horizontal speed coming from the GNSS receiver; ΔV_E is the speed mismatch; ε is the angular rate of the gyroscope drift; α is the stabilization error.

The dashed line in Fig. 1.15 shows the physical connections determining the measuring signals of the GP sensing elements.

The transfer function of the filter $F(p)$ has the following form:

$$F(p) = \frac{n^2}{2} \cdot \frac{2.6Tp + 1}{0.5Tp + 1},\ n = \frac{T_{Sch}}{T}, \tag{1.2.10}$$

where $T_{Sch} \approx 13.4$ min is the Schuler time constant, T is the response time of the gyro vertical.

In this scheme, the dynamic stabilization error during a maneuver is eliminated by subtracting the speed value received from the GNSS from the signal coming to the input of the filter $F(p)$. In addition, control signals equal to the projections of the Earth's angular rate on their sensitive axes are fed to the gyroscope torquers. At the same time, the difference between the speed components coming from the

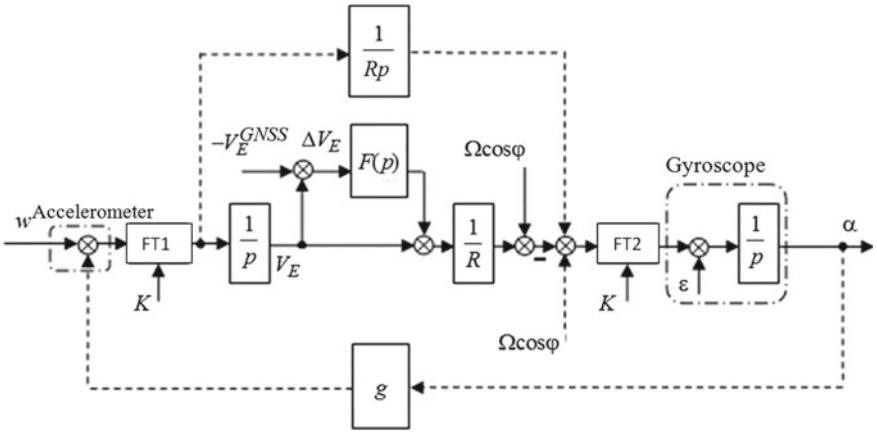

Fig. 1.15 Block diagram of the 'eastern' channel of the gyro vertical

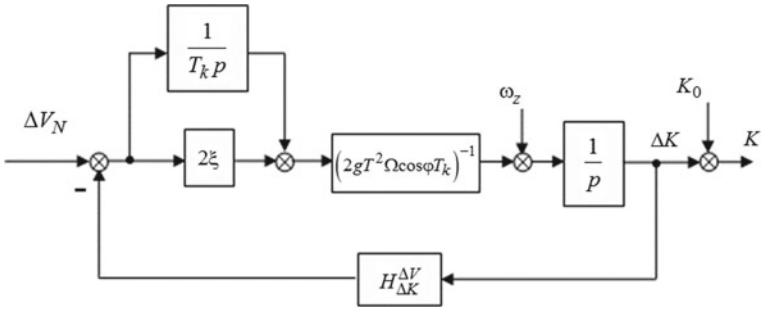

Fig. 1.16 Block diagram of the heading channel

GNSS receiver and those produced by the inertial method is formed in the axes of the geographic trihedron (FT1), and the control signals to the gyroscope torquers are formed in the instrument coordinate system (FT2). Thus, in the gyro vertical channels, the coordinates are converted twice based on the current values of the heading. The heading value can come from an external source or be generated autonomously based on the information from the fiber-optic angular rate sensor installed on the gyro platform and the angular rate error in the northern channel of the gyro vertical.

The analytical generation of heading is based on the gyrocompassing method using, in addition, the information from the azimuth FOG (Krasnov 2007). The block diagram of the heading channel is shown in Fig. 1.16.

The following symbols are used in the figure: T_k is the response time of the heading channel; ξ is the damping coefficient; ΔV_N is the mismatch of the northern component of the speed; ω_Z is the vertical angular velocity of the carrier according to FOG data; $H_{\Delta K}^{\Delta V}$ is the transfer function of the gyro vertical from the heading error to the speed mismatch; ΔK is the correction to the current heading value in the frame transformers.

Before the vehicle begins to move, the initial heading value K_0 is calculated and the FOG zero drift is specified. The heading is determined according to the formula:

$$K = \arctan \frac{\omega_y}{\omega_x}, \tag{1.2.11}$$

where ω_y, ω_x are the signals from the torquers of the floated gyroscope satisfying the following relations:

$$\begin{aligned} \omega_y &= \Omega \cos\varphi \sin K, \\ \omega_x &= \Omega \cos\varphi \cos K. \end{aligned} \tag{1.2.12}$$

In accordance with the principle of gyrocompassing, the feedback comes from the "northern" channel of the gyro vertical. The correction ΔK is formed by two signals, the mismatch of the northern speed component and the vertical angular rate from the FOG. The response time of the heading channel T_k is chosen at least an

order of magnitude greater than that of the gyro vertical T so that the gyro vertical errors will not participate in the formation of correction ΔK.

1.2.6 Calibration and Verification of the Chekan-AM Gravimeter

Calibration of the Chekan-AM gravimeter is performed during the manufacturing process. It includes the determination of the coefficients of the GSE calibration characteristic, its response time, and the value of the initial drift. The following GP parameters are also determined during calibration: scale factors and gyroscope drifts and accelerometer zero offsets, servo drive coefficients, and non-orthogonality of the floated gyroscope axes.

Since the Chekan-AM gravimeter is a certified measuring instrument, it also undergoes primary and periodic calibrations. The error components due to the influence of inertial accelerations and temperature are determined during the calibration.

Figure 1.17 shows a GSE calibration characteristic of a Chekan-AM mobile gravimeter. As Eq. (1.2.7) shows, it is a quadratic function whose coefficients are determined experimentally by the tilting method (Sokolov et al. 2015). The main feature of the method is the possibility to determine the coefficients only in the direction of decreasing gravity due to the GSE tilt. At the same time, the GSE is tilted by an angle of up to 5° with an error of less than 2 arcsec, which allows the device to be calibrated in the range of 0–4 Gal with the required accuracy. As can be seen from Fig. 1.17, the error due to the nonlinearity of the calibration characteristic does not exceed 0.2 mGal.

The next main parameter determined during the GSE calibration is the drift value. Taking into account the fact that the drift of the newly manufactured GES can reach from 3 mGal/day (the Chekan-AM gravimeter) to 1 mGal/day (the Shelf-E gravimeter), this step of calibration takes at least one month and is performed in

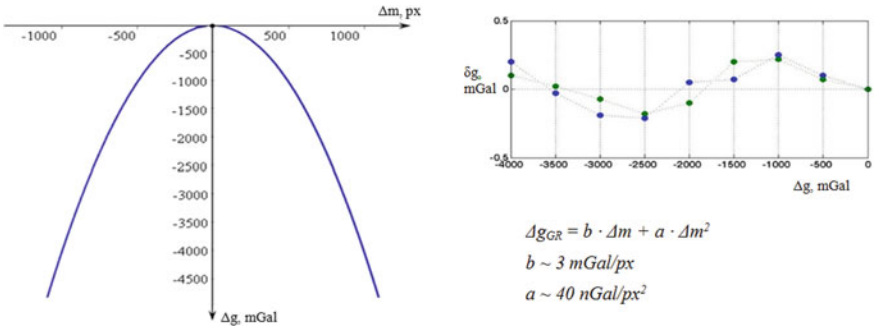

Fig. 1.17 Calibration characteristic and the error of its determination

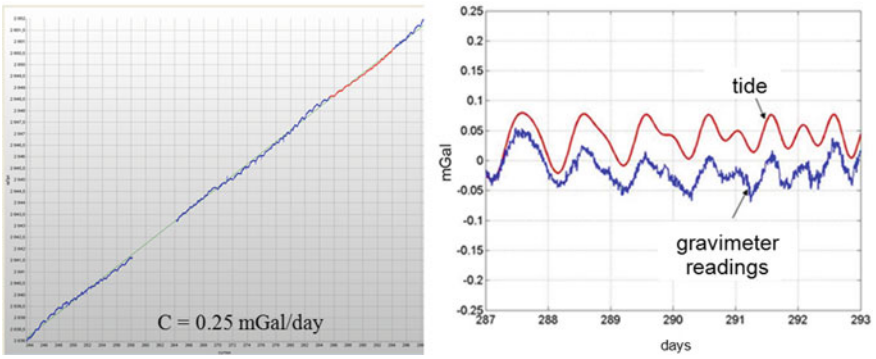

Fig. 1.18 GSE measurements on a fixed base

parallel with all types of tests. Figure 1.18 shows the curve of the Shelf-E drift two years after the GSE manufacture. It is obvious that in addition to a high degree of the drift linearity, its value is 0.25 mGal/day, which is almost 5 times lower than the initial value and is close to the similar parameters of the GT-2 and L&R gravimeters.

Removing the linear drift from the gravimeter readings, it is possible to qualitatively estimate its instrumental accuracy on a static base. An illustrative example of this is also given in Fig. 1.18 which shows that it is possible to observe lunar-solar tides whose influence on the change in gravity is less than 0.1 mGal.

Figure 1.19 shows the results of bench tests of the Chekan-AM and Shelf-E gravimeters when they were exposed to vertical accelerations in the range of periods from 14 to 100 s. The curves shown for the residual errors of the gravimeter readings were obtained after correction for the vertical acceleration, which was calculated based on the readings from the vertical displacement test bench, and data processing using a low-pass filter with a cutoff frequency of 0.006 Hz. The upper part of the figure shows the values of the amplitude and period of the vertical accelerations set for all modes of rocking. From the experimental data, it follows that the standard deviation of random error component of gravimeters in a wide range of frequencies of vertical accelerations does not exceed 0.2 mGal.

However, a systematic error, which may reach 1.5 mGal for the Chekan-AM gravimeter, is observed at high frequencies. For the Shelf-E gravimeter, this systematic error is three times lower. The reduction of the systematic error in the high-frequency range of vertical disturbing accelerations is due to a higher level of damping of the gravimeter sensing element. Owing to the digital filter used to recover the input signal, the increase in the damping level does not affect the final resolution of measurement results.

The effect of the ambient temperature variation on the Shelf-E gravimeter readings is shown in Fig. 1.20. It is obvious that in the operating temperature range between +5 to +35 °C, a 5° change in temperature results in a transient process with amplitude of up to 1 mGal, which lasts about 4 h. Besides, the steady-state systematic component of the error is significantly lower for the Shelf-E gravimeter than that for the Chekan-AM

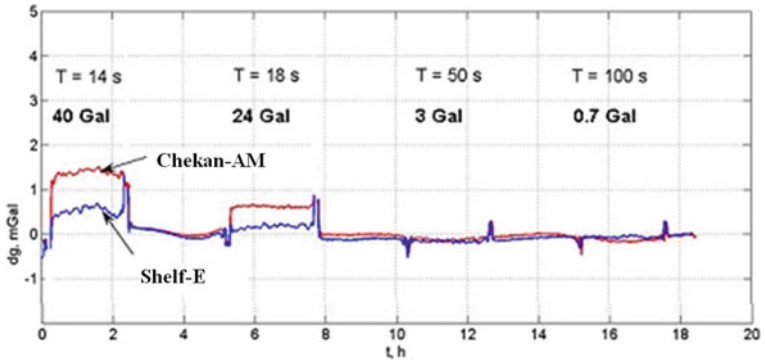

Fig. 1.19 Gravity measurements under the action of vertical accelerations

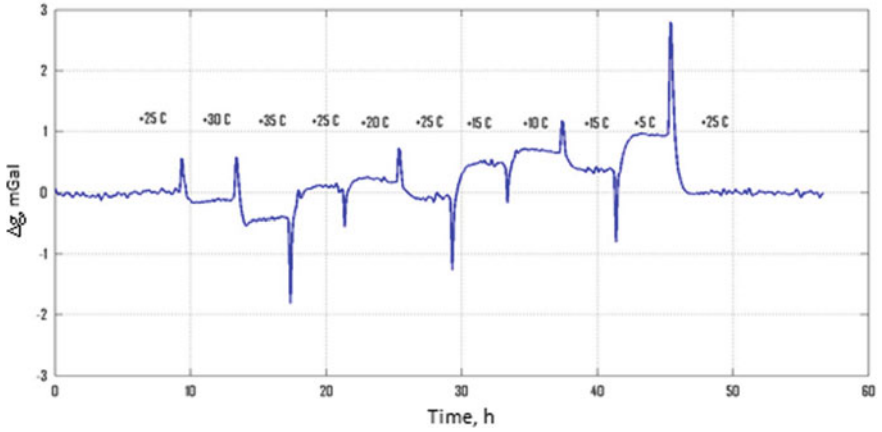

Fig. 1.20 Shelf-E gravimeter measurement error under the changes of ambient temperature

gravimeter. This is very important when conducting airborne gravity measurements, where daily external temperature differences may reach tens of degrees.

1.2.7 Conclusions

The main technical solutions implemented in the Chekan-AM mobile gravimeter, which is the fourth-generation system, have been described.

The main parts of the gravimeter, its structure, and the differences between the marine and airborne versions have been discussed.

The gravimeter sensing element and the gyro platform have been considered in detail, including the principle of operation, design features, mathematical models and operation algorithms.

The features of the Chekan-AM mobile gravimeter calibration have been discussed, and the main results of the bench tests are presented.

The advantages of the new Shelf-E system have been analyzed by comparison with the Chekan-AM gravimeter.

Gravimetric data processing methods and examples of the practical use of Chekan-AM in hard-to-reach areas of the Earth are given in the subsequent chapters.

1.3 GT-2 Relative Gravimeters

Gravimeters of the GT-2 series (GT-2A and GT-2 M are the codes for airborne and marine gravimeters, correspondingly) manufactured by NTP Gravimetric Technologies are widely used in gravity surveys aboard sea vessels and aircraft. More than 40 gravimeters of this series are used in gravity surveys of Russian and international companies on all continents of the Earth, including the Arctic and Antarctic regions (Richter et al. 2013; Berzhitsky et al. 2002; Kovrizhnykh et al. 2013a, b, 2016; Kovrizhnykh and Shagirov 2013; Smoller et al. 2013; Drobyshev et al. 2011; Mogilevsky et al. 2015a). Aerogeophysica Geophysical Scientific and Production Enterprise (Mogilevsky et al. 2010, 2015b; Kontarovich and Babayants 2011; Mogilevsky and Kontarovich 2011; Kontarovich 2015) and the Schmidt Institute of Physics of the Earth of the Russian Academy of Sciences (Koneshov et al. 2013; Drobyshev et al. 2011) that conduct a great number of airborne gravity surveys throughout Russia are the main Russian users of these airborne gravimeters. The GT-2 gravimeter was developed by a group of scientists and engineers at Gravimetric Technologies. The main designers of the company, who had been engaged in research and development at the Dolphin Central Research Institute for more than thirty years, specialized in developing inertial gravimetric systems and gyroscopic systems for the Russian Navy. Five technical solutions implemented in the gravimeter are recognized as inventions and protected by patents of the Russian Federation (Berzhitsky et al. 1999, 2000; Ilyin et al. 1993). The software for post-processing of airborne measurements for GT-2 gravimeters was developed in the Laboratory of Control and Navigation of the Lomonosov Moscow State University (Koneshov et al. 2013b). The first model of the GT-2 gravimeter was manufactured in 2001. It was tested aboard an AN-30 aircraft in Kubinka and in the vicinity of the Cherepovets airport. In 2002, the first commercial gravimeter was manufactured. With the financial support of Canadian Micro Gravity, it was put to extended tests in Australia on a plane, car, and helicopter, the results of which were considered positive. In February 2003, a long-term agreement was signed with Canadian Micro Gravity on the commercialization and supply of GT-2 gravimeters. Gravimeters of this series are manufactured in cooperation with the Ramensky Instrument-Making

Plant. At the stage of development, the plant carried out substantial work on preproduction engineering and revision of the documentation for the gravimeter central device to comply with the series-produced elementary base.

Gravimeters of this series are continuously improved. The first gravimeters, codenamed GT-1A, had a dynamic measuring range of ±0.5 g. In 2007, gravimeter versions with an extended dynamic range of ±1 g were created. They were assigned the codes of GT-2A, GT-2 M. The GT-2A, GT-2 M gravimeters allow conducting surveys in harsh conditions of strong turbulence and sea waves, which significantly increases the performance of survey. Actually, all gravimeters produced earlier were upgraded to this version.

In 2012, another version of the gravimeter with an extended latitude range of ±89° was created (a gravimeter with standard specifications has a latitude range of ±75°). The new gravimeter was equipped with a multi-antenna GNSS receiver. This version was assigned the code GT-2AP. It allows conducting surveys in high latitudes (Smoller et al. 2013; Drobyshev et al. 2011). In 2015, a version of the GT-2AQ gravimeter was created using quasi-coordinates.

This version has no restrictions on latitudes in its application. It retains its operability even directly at the points of geographic poles (Smoller et al. 2016). At present, three international companies—the University of Texas (USA), the Wagner Institute (Germany), and the Polar Research Institute of China—are conducting gravity surveys in the Antarctic using polar versions of the GT-2A gravimeter.

GT-2A gravimeters have high measurement accuracy. For the airborne version, it is between 0.5 and 0.7 mGal with an averaging time of 100 s, which, at an aircraft speed of 200–400 km/h, corresponds to the spatial resolution of half the anomaly length of 2.5 km to 5 km; for the marine version, 0.3 mGal with an averaging time of 600 s, which at a vessel speed of 5 kn corresponds to a spatial resolution of half the anomaly length of 0.75 km.

The higher averaging time for the marine version of the gravimeter as compared with the airborne version is due to the fact that the level of noise in the marine version is caused by sea swell and is significantly higher than that in the airborne version, which is caused by the GNSS error (for more details, see Sect. 2.4).

However, despite this, the resolution in the marine version is higher than that in the airborne version because of relatively low speeds of vessels.

1.3.1 Gravimeter Parts

The structure of the GT-2 gravimeter is shown in Fig. 1.21.

The gravimeter uses real-time information from a GNSS receiver operating in the standard mode.

Schematic of the GT-2 gravimeter is shown in Fig. 1.22.

The gravimeter includes a gyrostabilized platform in a triaxial gimbal suspension with an external azimuth axis (the motor of the azimuth axis is not shown).

The following equipment is installed on the platform:

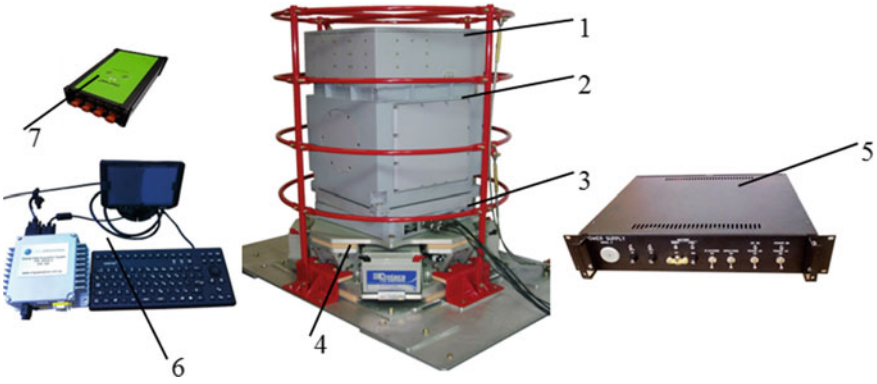

Fig. 1.21 Gravimeter structure: *1*—electronics module; *2*—central (gyro) module; *3*—rotary table; *4*—shock-absorber; *5*—power supply device; *6*—control and indication device (CID); *7*—GNSS receiver

- a GVK-18 dynamically tuned gyroscope (DTG) (Matveev et al. 2005) with a vertical orientation of the angular momentum, developed by Ramenskoye Instrument Design Bureau; the drift instability is 0.01–0.02°/h;
- two horizontal quartz pendulum-type accelerometers QAx, QAy of the A15 type developed by Ramenskoye Instrument Design Bureau with a zero signal instability of $5 \cdot 10^{-4}$ m/s^2;
- gravity sensing element (GSE);
- medium-grade FOG (Logozinsky, Solomatin 1996) developed by Fizoptika with a vertical sensitive axis, the drift instability of which during the entire period of operation without a thermal regulation system is 3°/h. Its short-term (within 5 to 10 days) drift instability in the gravimeter is 0.6°/h.

The output signals of accelerometers (W_x, W_y), GSEs (W_z), DTG angle sensors (β, γ), and FOGs (Ω_Z) are fed through the analog-to-digital converter (ADC) to the central processing unit (CPU) of the micro PC 5066 type. The DTG control signals (p_x, q_y) generated in the CPU by the gyro platform position correction system are fed through digital-to-analog converters (DAC) to the DTG torquers.

The control signals M_x, M_y of the servo drives generated in the CPU are fed through a DAC to the torque motors TM_x, TM_y of the servo drives.

The azimuthal stabilization motor control signal generated in the CPU according to the gyro platform heading information is fed to an azimuth stabilization motor (not shown in the figure), which ensures the platform stabilization in the geodetic reference frame.

GSE output signals are formed by an ADC with a range of +/–1 g.

To measure the angles of pitch, roll, and heading of the vehicle, angle sensors AS_x, AS_y, AS_z are installed on the axes of the gimbal suspension and on the vertical axis of the rotary table.

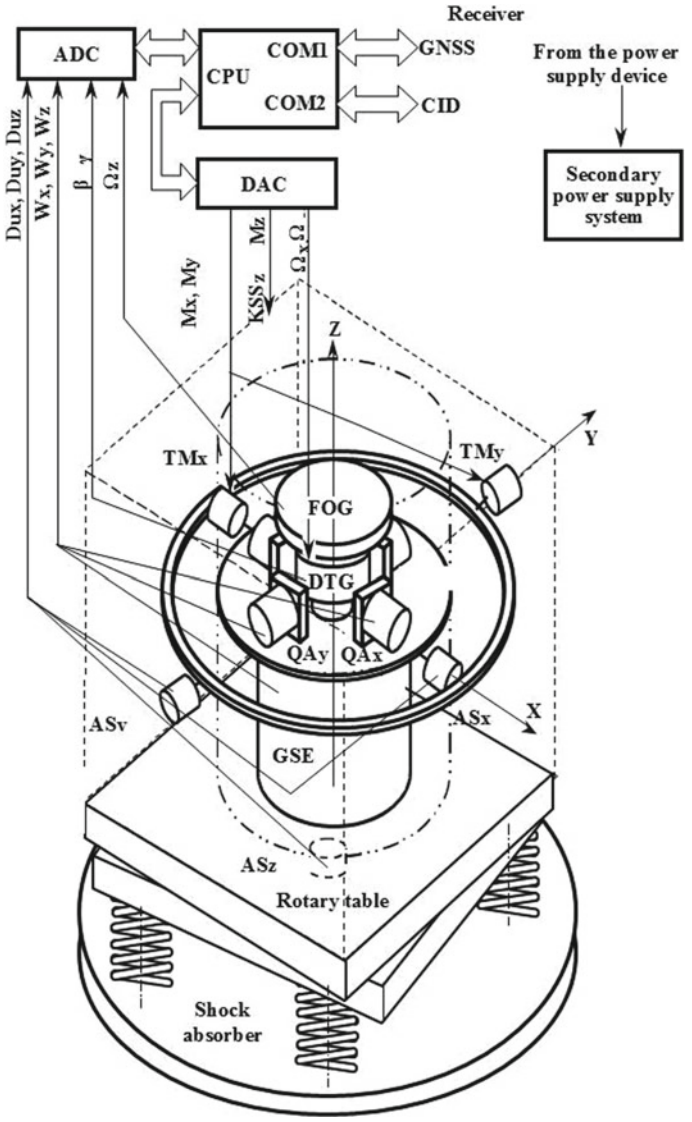

Fig. 1.22 Schematic of the GT-2 gravimeter

To ensure a constant temperature of the sensing elements, the code-to-current converter (CCC) for controlling the DTG torquers during fluctuations in the ambient temperature, the thermal regulation systems (TRS) include:

- single-circuit TRS of the CCC;
- single-circuit TRS of the inertial module with DTGs, FOGs, and accelerometers;
- dual-circuit GSE TRS.

The TRS actuating elements are controlled by the CPU using thermal bridge signals that are fed to the DAC via analog-to-digital converters.

1.3.2 Gravimeter Sensing Element

The sensing element of the GT-2 gravimeter is of the axial type with a magnetoelectric feedback. Its block diagram is presented in Fig. 1.23.

Proof mass (about 37 g) is suspended on flat metal springs with a thickness of about 50 μm. The measuring winding placed in a permanent magnet field is wound on the proof mass. The GSE includes an optical position sensor consisting of light and photo diodes. The sensor measures the proof mass displacement relative to the housing, and hence its displacement in the magnetic field of permanent magnets. The signal from the photo diode passes through a correction amplifier with a transfer function $F(s)$ that provides stable feedback and changes the current in the measuring winding. A precision reference resistor R is connected in series with the winding. The current in the measuring winding, and hence the voltage across the resistor R, is a measure of the specific force projection onto the GSE sensitive axis (W_z). The signal proportional to the voltage on the reference resistor, as well as the output signal of the position sensor enter the CPU via analog-to-digital converters.

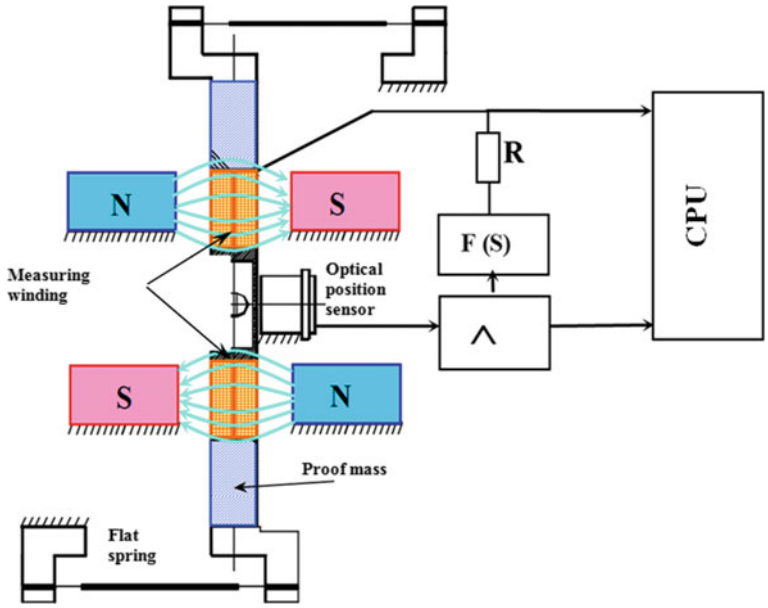

Fig. 1.23 Block diagram of the gravimeter sensing element

The feedback, which stabilizes the proof mass position relative to the housing, is based on an analog circuit. When there is no vibration, the proof mass is practically immobile relative to the GSE housing, and hence, relative to the magnetic field generated by the magnetic system. Under vibration, the proof mass moves relative to the magnetic field. The averaged data of the GSE have an error proportional to the square of the proof mass deviation from zero, which is due to the nonlinearity of the magnetic field mainly caused by the error in the geometry of the permanent magnets and the displacement of the initial position of the proof mass relative to the magnets The proportionality coefficient K_{ps} is determined at the manufacturing plant when the gravimeter is calibrated on a vibration table and is used in the mathematical software of the gravimeter to compensate for the effect of the proof mass deviation on the GSE readings.

The block diagram of an axial-type GSE has an advantage over a pendulum-type GSE: it has no cross-coupling effect error (Dehlinger 1978). However, due to the finite longitudinal rigidity of the spring plane, the averaged data of the GSE have an error proportional to the square of the horizontal acceleration. The proportionality coefficients $K w_x(y)$ are determined at the manufacturing plant when the gravimeter is calibrated on a horizontal acceleration test bench and are used in the firmware of the gravimeter to compensate for the GSE error caused by the square of the horizontal accelerations.

GSE bandwidth is from 0 to 100 Hz. The measuring range is ±1 g. The drift is ±3 mGal/month. The standard deviation of the noise component in the test bench conditions is ±0.1 mGal to 0.2 mGal with an averaging time of 60 s.

1.3.3 Circuit for Integrated Correction of the Gyro Platform Position

The gravimeter has a Schuler-type circuit for integrated correction of the gyro platform position.

A block diagram of one channel of the correction circuit is shown in Fig. 1.24. The dead reckoning equations are integrated in the azimuth-free coordinate system. The azimuth-free coordinate system is determined by the *XaYaZa* frame-of-reference (Fig. 1.25) obtained from the local geodetic reference frame *ENZ* by turning around the vertical axis *Z* and having a zero component of the absolute angular rate with respect to the vertical axis *Za.*

The following symbols are used in the figure:

a_y is a projection of the horizontal specific force of the aircraft on the instrument axis Y (see Fig. 1.25);

W_x, W_y are readings of the accelerometers *X* and *Y*, respectively;

$\widehat{dw}_x$, $\widehat{dw}_y$ are estimates of biases of the transducer accelerometers (see Fig. 1.27); scale-factor errors are not taken into consideration;

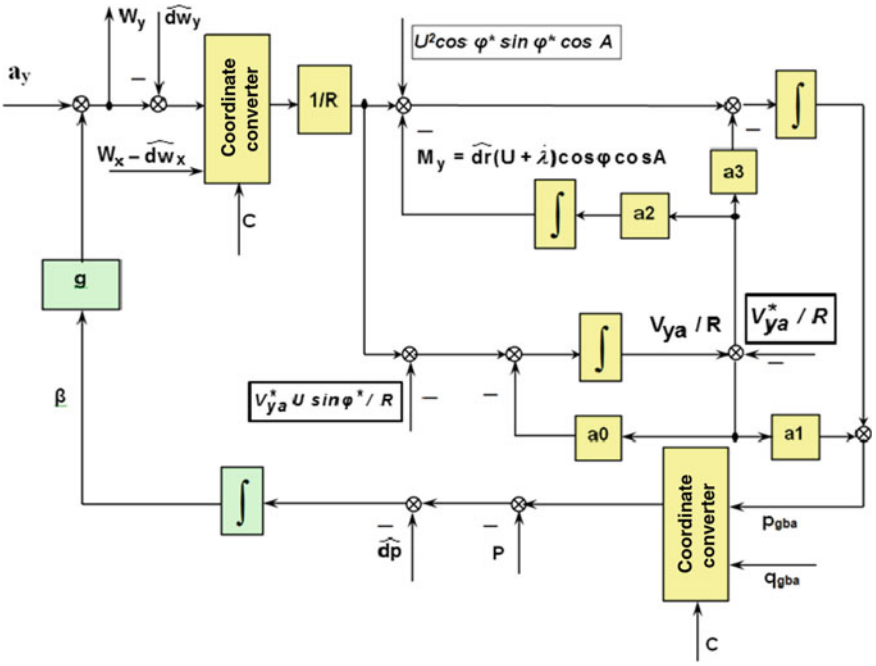

Fig. 1.24 One channel of the circuit for integrated correction of the gyro platform position

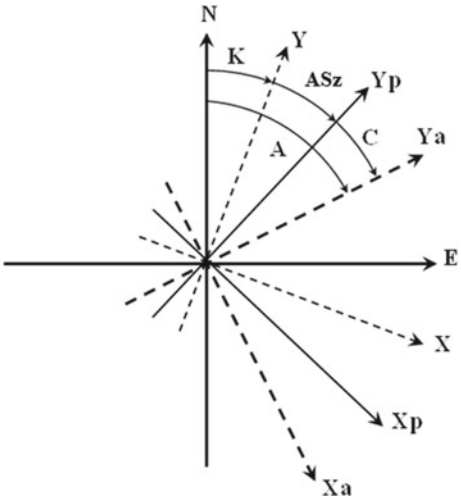

Fig. 1.25 Coordinate systems

C is the angle between the platform coordinate system and the azimuth-free coordinate system (see Fig. 1.25);

g is the absolute value of gravity on the flight path;

$\widehat{dr}$ is an estimate of the angular rate of the FOG drift;

R is the mean Earth radius;

φ is the geographical latitude of a point;

$\dot{\lambda}$ is the longitude derivative;

U is the absolute value of the Earth's angular rate;

β is the misalignment error of the gyro platform around the X axis;

A is the heading of the azimuth-free coordinate system (see Fig. 1.25);

p_{gba}, q_{gba} are the signals applied to the DTG torquers, in projections on the Xa and Ya axes of the azimuth-free coordinate system (see Fig. 1.25);

P is the projection of the absolute angular rate of the gyro platform on the X_p axis of reference frame whose azimuthal orientation is determined by the angle of the platform heading (see Fig. 1.25);

$\widehat{dp}$ is an estimate of the drift angular rate of the DTG and the transducer around the X axis (see Fig. 1.29), errors of the scale factors are not considered;

V_{xa}, V_{ya} are projections of the relative velocity of the vehicle on the Xa and Ya axes of the azimuth-free coordinate system (see Fig. 1.25);

$a0 - a3$ are the coefficients of gyro platform oscillation damping algorithm:

$$\begin{aligned} a0 &= 2.613/T_{gg}; \\ a1 &= 1 - 3.414/\upsilon^2; \\ a2 &= \frac{-1}{\upsilon^2 T_{gg}^4}; \\ a3 &= a0\left(1 - \frac{1}{\upsilon^2 T_{gg}^2}\right); \end{aligned} \tag{1.3.1}$$

υ is the Schuler frequency;

T_{gg} is a parameter corresponding to the time constant of the gyro platform position correction system.

The Schuler-type integrated correction circuit of the gyro platform nondisturbed by the vehicle motion (Seleznev 1967) was synthesized based on the equations of the stationary Kalman filter (KF). The following simplifications were accepted for the relevant algorithmic solutions: channel-by-channel models of the INS error equations are used; the FOG drift is considered as the integral of white noise; and white noise is considered as a statistical approximation of the error in the GNSS-derived velocity (Smoller 2002). This led to an easy-to-operate and easy-to-customize one-parameter algorithmic structure, the parameters $a0$, $a1$, $a2$, $a3$ of which—the damping coefficients (1.3.1)—are a function of one parameter, T_{gg}. Application of the algorithm for damping gyro platform angular oscillations using the GNSS-derived velocity made it possible to ensure the value of the misalignment errors in the instrument leveling during the flight at a level of 1–2 arcmin. The misalignment errors of the instrument

leveling are estimated at the stage of integrated postprocessing of airborne gravimetric data using the GTNAV software (see Sect. 1.2.2). In the GTNAV software, estimation of misalignment errors is carried out with the use of the smoothing KF, which is based on sufficiently complete models of INS error equations and models of instrumental errors of inertial sensors. Measurements are formed with the use of GNSS differential carrier phase solutions. This allowed providing the level of 10–15 arcsec for errors in estimating the misalignment errors of the vertical, which is confirmed by the experience in processing experimental data.

In Fig. 1.24, the formulas that use aiding information are shown in italic and are framed for clarity. Symbol * indicates trajectory parameters provided by the GNSS. The upper formula is a compensation for the gyro platform misalignment error due to the centripetal acceleration caused by the Earth's rotation, the lower one is a compensation for the Coriolis acceleration projection on the vertical axis, and the right one is the aiding data used to damp gyro platform oscillations. The GNSS receiver delivers the values of the aircraft velocity vector components in projections on the axes of the geographic coordinate system with the axes oriented according to the sides of the world (east, north) and upwards (*ENZ*). To implement the damping algorithm, it is required to have external information about the vehicle velocity on the axis of the azimuth-free geographical coordinate system. When calculating the velocity projections, it is necessary to know the heading angle. Significant errors in external information can result from the heading errors.

Coordinate Systems. Main Formulas. Figure 1.25 shows the main coordinate systems used in the gravimeter software.

For simplicity, let us assume that the roll and pitch of the aircraft are equal to zero and the gyro platform is not disturbed. Figure 1.25 shows the horizontal axes of the four coordinate systems. The vertical axes of all the coordinate systems considered are directed perpendicular to the plane of the drawing to the observer.

The following symbols are used in the figure:

E, N are the axes of the geographic reference frame;

X, Y are the aircraft body frame axes;

Xp, Yp are the gyro platform axes;

Xa, Ya are the axes of the azimuth-free coordinate system;

K is the vehicle heading;

A is the heading of the azimuth-free coordinate system;

AS_z is the readings of the angle sensor of the gimbal suspension external axis;

C is the angle between the platform coordinate system and the azimuth-free coordinate system calculated by integrating the FOG readings (r):

$$C = \int r dt. \tag{1.3.2}$$

The standard-configuration GT-2 gravimeter uses the data from a single-antenna GNSS receiver for damping of the gyro platform. The GNSS receiver (both single-antenna and multi-antenna) initially determines the coordinates and projections of the relative velocity vector in the Greenwich coordinate system, then recalculates them

into the geodetic reference frame *ENZ* (for more details, see Sect. 4.3). The single-antenna GNSS receiver provides the geographic coordinates (latitude and longitude), the aircraft relative velocity vector projection V^* onto the local horizon plane and the track angle TA*, which is the angle between the projection of the above-mentioned vector onto the horizon plane and the north direction.

In the standard configuration, heading A of the azimuth-free coordinate system, as well as the velocity projections V_{xa}^*, V_{ya}^*, necessary for damping of gyro platform oscillations (see the formulas given in italics and framed in Fig. 1.24), are calculated in the GT-2 gravimeter software based on the following formulas:

$$\begin{aligned} U_{xa} &= p_{gba} - V_{ya}^*/R; \\ U_{ya} &= q_{gba} - V_{xa}^*/R; \end{aligned} \tag{1.3.3}$$

$$A = arctg\left(U_{xa}/U_{ya}\right); \tag{1.3.4}$$

$$V_N^* = V^* \cos TA^* + V^* \sin TA^*; \tag{1.3.5}$$

$$V_{ya}^* = V_N^* \cos A + V_E^* \sin A; \tag{1.3.6}$$

$$V_{xa}^* = V_E^* \cos A - V_N^* \sin A. \tag{1.3.7}$$

In formulas 1.3.3, U_{xa}, U_{ya} represent the calculated values of the Earth's angular rate projections onto the corresponding axes in the azimuth-free coordinate system. The heading calculated from formulas (1.3.3, 1.3.4) is called a compass heading. As is known (Smoller et al. 2015), the error in the calculation of the compass heading is expressed by the following formula:

$$dA = \frac{dp_E + \dot{\beta}_E}{\left(U + \dot{\lambda}\right)\cos\varphi}, \tag{1.3.8}$$

where dp_E is the east drift of the DTG;
$\dot{\beta}_E$ is the dynamic error rate of the gyro horizon around the eastern axis;
$\dot{\lambda}$ is the longitude derivative.
Analysis of formula (1.3.8) allows for the following conclusions:

1. As latitudes φ become higher, heading error A in the single-antenna configuration of the gravimeter, and hence, relevant induced errors in determining the relative velocity components V_{xa}^*, V_{ya}^* required for damping increase in (1.3.6, 1.3.7). When approaching the pole, the value dA tends to infinity. This makes it impossible to use the GT-2A gravimeter at latitudes higher than $\pm$ 75°.
2. Flights in the eastward direction in terms of the heading error, when the value $\dot{\lambda}$ is positive, are preferable to flights in the westward direction, when the value

$\dot{\lambda}$ is negative. This effect is particularly significant at high latitudes, where the value $\dot{\lambda}$ becomes commensurate with the angular rate of Earth's rotation U.

3. The heading error dA in the standard single-antenna gravimeter configuration depends on the instability of the instrumental errors of the inertial gravimeter sensing elements, which cause misalignment errors of the gyro platform and on the constant eastern drift of the DTG. The compass heading error does not depend on the constant component of the FOG drift.

An alternative to the compass heading in the GT-2A gravimeter could be the inertial heading A_i calculated by the formula:

$$A_i = \int (r - (U + V_E^*/R\cos\varphi^*)dt + A_i(0). \tag{1.3.9}$$

By varying this relation under the assumption that the FOG drift dr is a constant and neglecting the GNSS errors, we obtain

$$dA = dr \cdot t. \tag{1.3.10}$$

The comparison of the compass heading error (1.3.8) with the inertial one (1.3.10) allows for the following conclusion: the inertial heading has no distinguishing features at high latitudes, but it cannot be used in the GT-2 gravimeter because of the medium-grade FOG. As mentioned in Sect. 1.3.1, its short-term instability is 0.6°/h, which in 5 to 10 h flights can lead to an unacceptable inertial heading error of (3–6)°, while the GT-2 gravimeter compass heading error does not exceed 0.5–1°. To eliminate the features of the compass heading, it was proposed to use a multi-antenna GNSS receiver. The main idea of its use is that the multi-antenna GNSS receiver generates the value of the carrier heading in addition to navigation information, in particular, the relative velocity and the local coordinates. The heading obtained in this way has no drawbacks that are inherent in the compass heading obtained in the standard configuration of the GT-2A gravimeter. Thus, by using the readings from the angle sensors of gravimeter gimbal suspension, it becomes possible to determine the projections of the carrier relative velocity vector on the gyro platform axes, needed to damp oscillations of the gyro platform. This circumstance, as well as the use of quasi-coordinates in the software of the gravimeter and GNSS receiver, made it possible to create an all-latitude version of the GT-2AQ gravimeter. Creating an all-latitude version of the gravimeter is discussed in Sect. 4.3.

1.3.4 Mathematical Models of the Channels of Inertial Sensing Elements

The term 'channels' of the GSE, FOG, and horizontal accelerometer is used to mean the mathematical model of these inertial sensing elements with an integrating ADC and a sequence of computations in the CPU for the purpose of compensation for systematic instrumental errors and digitization of the output signal in the appropriate dimension. The concept of the DTG channel is defined below.

Gyro Platform Channel of the Gravity Sensing Element

Figure 1.26 on the left shows the adopted mathematical model of a GSE with an ADC; on the right, mathematical calculations implemented in the CPU.

The following symbols are used in Fig. 1.26:

W_z is the vertical specific force (for simplicity, it is assumed that the QA sensitive axis coincides with vertical);

Kw_z is the scale factor error of a transducer GSE;

dw_z is the zero signal drift of a transducer GSE;

$\widehat{Kw}_z$ is an estimate of the error of the scale factor of a transducer GSE;

$\widehat{dw}_z$ is an estimate of the zero signal drift of a transducer GSE;

T_e is the anti-alias filter time constant;

W_{zout} is the GSE channel output data.

The GSE signal is read out at a frequency of 300 Hz by an integrating ADC, at the output of which the average value of acceleration is in the range of 1/300 s. After the scale factor error $\widehat{Kw}_z$ compensation and the zero signal drift $\widehat{dw}_z$, the data obtained is passed through an anti-aliasing filter (aperiodic link with the time constant $T_e = 2$ s). Its output is averaged over 16 readings. The values W_{zout} W_{zout} with a frequency of about 18 Hz (more precisely, 300/16 Hz) are recorded in the G file and fed to the input of the vertical channel generating gravity anomalies in the GT-2 M marine gravimeter. In the GT-2A airborne version, the output data of the vertical channel are used when the aircraft is for functional diagnostics at the airdrome.

It is easy to show that the impact of vibration on a gravimeter with a frequency close to the sampling frequency W_{zout} in the G file (approximately 18 Hz) leads to the effect of frequency masking and, consequently, to an undesirable low frequency in the output data of the GSE channel, which will be perceived as a false anomaly. The task of the anti-aliasing filter operating at 300 Hz frequency is designed to suppress

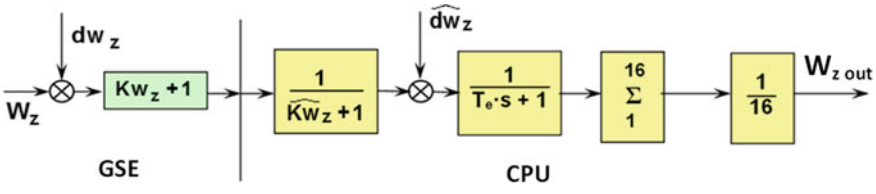

Fig. 1.26 Mathematical model of the GSE channel

the amplitudes of signals with frequencies close to 18 Hz. The use of an aperiodic link with the time constant $T_e = 2$ s as an anti-aliasing filter attenuates the amplitudes of the harmonics with frequencies close to 18 Hz by more than 200 times, which almost completely eliminates the effect of frequency masking. The anti-aliasing filter leads to a delay in the output data for a fixed time of 2 s, which is taken into account during postprocessing.

The value of the scale factor error for a transducer GSE is determined only at the instrument making plant during the manufacture of the gravimeter by the tilting method on a precision tilt meter device with a relative error not exceeding several 10^{-4}. More than a decade-long experience with operating gravimeters has shown that the value Kw_z remains stable with the specified accuracy throughout the entire period of operation.

Horizontal Accelerometer Channel

The following symbols are used in Fig. 1.27:

W is the horizontal specific force of the vehicle (for simplicity, it is assumed that the GSE sensitive axis coincides with vertical);

Kw is the scale factor error of a transducer accelerometer;

dw is the zero signal drift of a transducer accelerometer channel;

$\widehat{Kw}$ is the estimate of the scale factor error of a transducer accelerometer;

$\widehat{dw}$ is the estimate of the zero signal drift of a transducer accelerometer;

$\mathrm{W_{out}}\,W_{out}$ is the output signal of the accelerometer channel.

Figure 1.27 on the left shows the adopted mathematical model of a transducer accelerometer. The figure on the right shows the mathematical operations used to compensate for the factory-defined values Kw and dw. Obviously, in the ideal case of ($\widehat{Kw} = Kw, \widehat{dw} = dw$), the output signal of the accelerometer channel $\mathrm{W_{out}}\,W_{out}$ will be equal to the input acceleration W. The analog signal of the accelerometer with a frequency of 300 Hz is converted into a code by an integrating ADC. Thus, the CPU receives a code proportional to the mean value of specific force (specific velocity increment) over an interval of 1/300 s.

Practice has shown that Kw remains unchanged during operation with sufficient relative accuracy (not worse than 10^{-3}). The values $\widehat{Kw}_x$, $\widehat{Kw}_y$ are defined by the "Calibration" procedure (see Sect. 1.3.6) at the instrument making plant during the gravimeter manufacturing process. The values $\widehat{dw}_x$, $\widehat{dw}_y$ are also defined only at the instrument making plant during the gravimeter manufacturing as described in Sect. 1.3.5. The values $\widehat{Kw}_x(y)$ and $\widehat{dw}_x(y)$ discussed above are entered into the gravimeter database and remain unchanged during the entire period of operation.

FOG Channel

The following symbols are used in Fig. 1.28:

r is the vertical angular rate of the gyro platform;

Kr is the scale factor error of a transducer FOG;

dr is the zero signal drift of a transducer FOG channel;

$\widehat{Kr}$ is an estimate of the error of the scale factor of a transducer GSE;

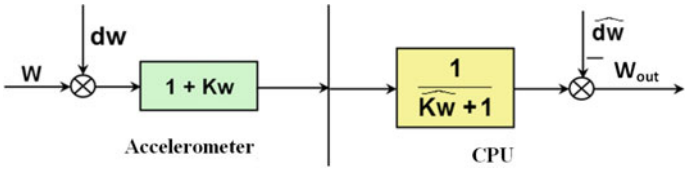

Fig. 1.27 Mathematical model of the accelerometer channel

$\widehat{dr}$ is an estimate of the zero signal drift of a transducer accelerometer;
r_{out} is the FOG channel output signal.

Figure 1.28 on the left shows the adopted mathematical model a transducer FOG. On the right, the figure shows the mathematical operations to compensate for the factory-defined values Kr and dr. It is obvious that in the ideal case ($\widehat{Kr} = Kr$, $\widehat{dr} = dr$) the output value of the FOG channel r_{out} will be equal to the input angular rate r. The analog signal of the FOG with a frequency of 300 Hz is converted into a code by an integrating ADC. Thus, the CPU receives a code proportional to the average value on an interval of 1/300 with the vertical angular rate of the gyro platform.

Practice has shown that the Kr value with sufficient relative accuracy (not worse than 10^{-3}) remains unchanged during operation. Therefore, Kr is determined by turning the platform of the gravimeter at a fixed angle using a rotary table and comparing the integral of r_{out} with its value. The dr value is determined occasionally, once every 10–15 days and after each cold start of the gravimeter during operation, using the automatic 'Autocalibration' procedure integrated in the gravimeter software (see Sect. 1.3.6).

The DTG, which is a free gyroscope, contains two torquers—X and Y—that provide precession movement of the gyro platform around horizontal axes. The input of the gyroscope is the magnitude of the current supplied by the code-to-current converter (CCC) to its torquer sensor winding, its output is the precession rate of its rotor, and hence the gyro platform, around the corresponding horizontal axis.

The DTG channel will be understood as a mathematical model of the DTG with a CCC and a sequence of computations in the CPU to compensate for systematic instrumental errors.

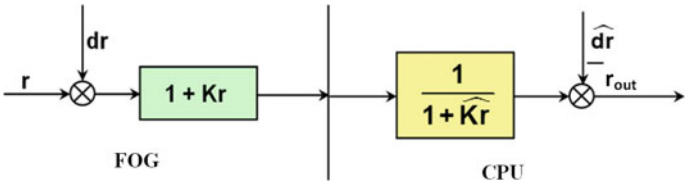

Fig. 1.28 Mathematical model of the FOG channel

One Channel of a Dynamically Tuned Gyroscope

The following symbols are used in Fig. 1.29:

p_{out} is the actual angular rate of the gyro platform around the X axis (for clarity, one of the identical X channels of the DTG is considered);

p is the angular rate of the gyro platform around the X axis fed to the input of the CCC (calculated by the correction system);

Kp is the scale factor error of the DTG and the converter;

dp is the angular rate component of the gyroscope drift around the X axis;

$\widehat{Kp}$ is an estimate of the scale factor error of the DTG and the converter;

$\widehat{dp}$ is an estimate of the angular rate of the DTG and transducer around the X axis.

Figure 1.29 on the right shows a mathematical model of the DTG and the CCC. On the left, the figure shows mathematical operations to compensate for the $\widehat{Kp}$ and $\widehat{dp}$ values determined during calibration. Obviously, in the ideal case ($\widehat{Kp} = Kp$, $\widehat{dp} = dp$), the actual angular rate of the platform p_{out} will have the design value of p.

Practice has shown that the Kp value remains unchanged during operation with sufficient relative accuracy (not worse than 10^{-3}). The values $\widehat{Kp}$ and $\widehat{dp}$ are defined at the instrument making plant in the process of gravimeter manufacturing by turning the gravimeter platform placed on a rotary table by four rhumbs relative to the meridian. The dp value is determined occasionally, once every 10–15 days and after each cold start of the gravimeter during operation, using the "Autocalibration" procedure integrated in the gravimeter software.

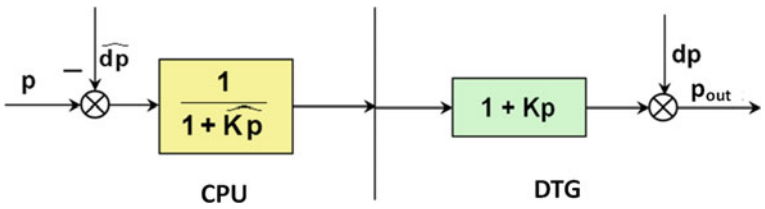

Fig. 1.29 DTG mathematical model and channel

1.3.5 Analysis of the Gravimeter Main Errors

Below is the main gravimetric equation which represents the GSE readings taking into account the gyro platform misalignment errors, geometry errors, and the instrumental errors taking into consideration the specific design features of the GT-2 gravimeter:

$$W_z = \left(\Delta g + g_0 + \Delta g_E + \ddot{Z}\right)\cos(\beta_Z + \alpha_1)\cos(\gamma_Z + \alpha_2) - W_y(\beta_Z + \alpha_1) + \\ + W_x(\gamma_Z + \alpha_2) + K_{PS} \cdot PS^2 + Kw_x \times Wx^2 + Kw_y \times Wy^2 + \upsilon,$$
$$g_0 = g_e - Wzz \cdot h, \tag{1.3.11}$$

where

W_z is the vertical specific force measured by a GSE;

Δg is the gravity anomaly;

g_0 is the normal gravity on the flight lines;

g_e is the normal gravity on the surface of the Earth's ellipsoid;

Δg_E is the Eötvös correction term;

$\ddot{Z}$ is the second derivative of the flight altitude;

β_Z is misalignment of the GSE sensitive axis of the gyro platform plane, which corresponds to the rotation around the *X*-axis;

γ_Z is misalignment of the GSE sensitive axis of the gyro platform plane, which corresponds to the rotation around the *Y*-axis;

α_1 is the misalignment of the platform caused by its disturbed state, which corresponds to the the rotation around the *X*- axis of the gyro platform;

α_2 is misalignment of the platform caused by its disturbed state, which corresponds to the the rotation around the *Y*-axis of the gyro platform;

W_x, W_y is the horizontal specific force of the carrier in projections on the *X* and *Y* axes, respectively measured by horizontal accelerometers;

K_{PS} is the coefficient of influence of the proof mass displacement relative to GSE housing caused by vibration on the GSE error;

PS is the readings of the GSE proof mass position sensor (see Fig. 1.3.3);

Kw_x, Kw_y are coefficients of influence of the horizontal projections of the vehicle acceleration in projections on the *X* and *Y* axes of the gyro platform, respectively, on the GSE error;

υ is random noise;

W_{ZZ} is the vertical gravitational gradient;

h is the flight altitude.

The plane of the gyro platform is a conditional concept defined by accelerometer signals. Let us assume that the plane of the platform coincides with the plane of the local horizon, when the accelerometer signals are equal to zero. Therefore, in the case of biases of the horizontal accelerometers, the values of β_Z, γ_Z will change.

As mentioned in Sect. 1.3.2, the influence coefficients of the proof-mass displacement relative to the GSE housing caused by vibration, and the influence coefficients of horizontal accelerations K_{PS}, $Kw_x(y)$ are determined at the manufacturing plant. They are entered into the gravimeter database and taken into account in real

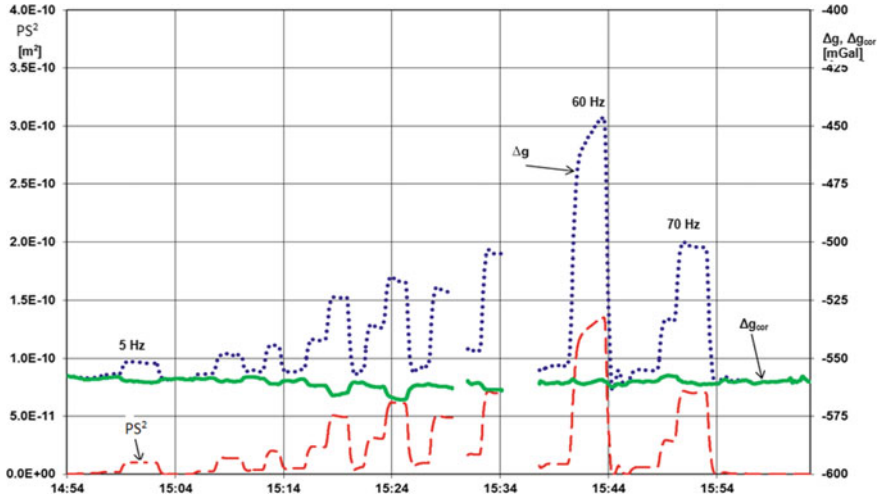

Fig. 1.30 Determination of K_{PS} on a vibration table

time to form corrections in accordance with the fourth, fifth, and sixth terms of formula (1.3.11), which practically eliminates the effect of vibration and horizontal accelerations of the vehicle on the gravimeter error.

Figure 1.30 shows an example of determination of the influence coefficient K_{PS} on a vibration table.

To identify the effect of the GSE proof-mass displacement during gravimeter calibration, vibration is set in the range from 5 to 70 Hz with amplitudes (0.2–0.3) g that are significantly higher than the vibration amplitudes acting on the gravimeter during the flight. The square of the deviation of the proof mass PS^2 [m^2] is shown by the dashed curve, the GSE readings are shown by the dotted curve. From these results, coefficient K_{PS} was determined as the ratio of the data of the dotted curve to those of the dashed curve. The result after the compensation is represented by the solid curve. From the curves presented, it follows that after the compensation, the effect of vibration decreased by more than 20 times.

Requirements for the accuracy of flight altitude determination. For simplicity, consider the following example.

Assume that the aircraft or, more precisely, a GSE proof mass is making vertical harmonic motion with an amplitude of $A = 1$ mm and a period $T = 100$ s (typical averaging time used in postprocessing of the GT-2A gravimeter measurements). The angular frequency $\omega \approx 0.061/s$. Assume that the GNSS receiver does not measure this displacement.

Then, in accordance with the first term of formula 1.3.11, there arises an error in the gravity anomaly generation with amplitude $d\Delta g$ equal to $\Delta g = \ddot{Z}_{max} = A\omega^2 =$ 0.4 mGal will appear. It follows that the accuracy of measuring the altitude of the GSE location should be approximately 1 mm (average for 100 s). As the experience with the operation of the GT-2A gravimeter has shown, this accuracy is achieved due

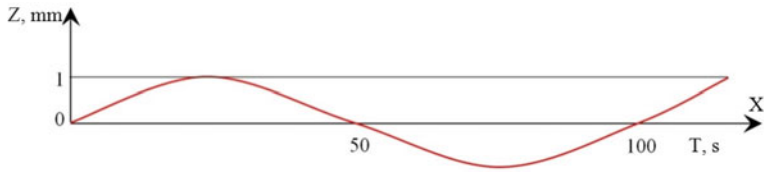

Fig. 1.31 The aircraft flight path leading to an error of 0.4 mGal

to the use of dual-frequency carrier phase GNSS receiver operating in the differential mode and with compensation of antenna lever arm effect using the readings from the angle sensors of the gravimeter gimbal suspension (Fig. 1.31).

Requirements for data synchronization accuracy. During the gravity survey, the data obtained from the GSE are recorded in the measuring file of the gravimeter. The GNSS data file obtained after taking into account the differential correction from the base station (hence, after the flight) is used to remove inertial perturbation from the GSE data. The data provided by GT-2 instrument should be time-synchronized. Let us estimate the requirement for data synchronization accuracy requirement using a simple example.

Assume that the aircraft is performing harmonic motion in the vertical plane ("GSE motion" curve in Fig. 1.32) with an amplitude $A = 1$ m and a period of 100 s (angular frequency $\omega \approx 0.061/s.$). Suppose that the GSE measurements ("GSE data" curve in Fig. 1.32) are ideal and the vertical acceleration is ideally determined using GNSS data ("GNSS" curve in Fig. 1.32), but the files have time lag relative to each other by $dt = 0.01$ s.

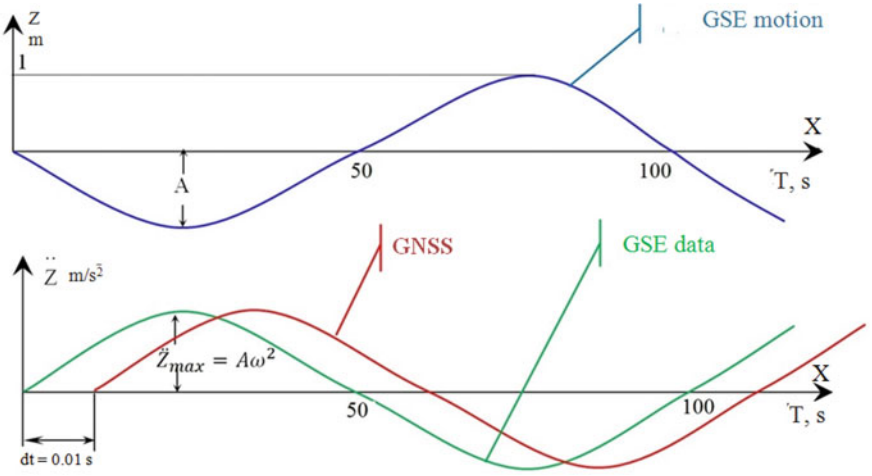

Fig. 1.32 Inaccuracy in synchronization between the GNSS and GSE data streams leads to an error of 0.2 mGal

It is easy to show that in this case, there will be an error in the gravity anomaly measurement with amplitude $d\Delta g$ equal to $d\Delta g = A\omega^3 dt \approx 0.2$ mGal .

It follows that the synchronization accuracy for the files should be at a level of 0.01–0.02 s (10– 20 ms).

In the GT-2A gravimeter, these requirements can be fulfilled owing to the following technical solutions:

1. Almost inertialess GSE with a bandwidth of 100 Hz is used, which corresponds to a GSE time constant of approximately 1 ms. Therefore, the GSE constant time and its instability during operation may be neglected.
2. GNSS-derived PPS signal, associated with the beginning of the Greenwich second, makes it possible to synchronise GSE measurements to an almost perfect accuracy of 0.00003 s (0.03 ms). For this purpose, the lag time of each individual GSE measurement from the PPS is recorded in the GSE file.

Requirements for the accuracy of the GSE-sensitive axis verticalization. There are two components of the GSE sensitive axis misalignment from vertical (the error in knowing the angle between the GSE sensitive axis and the vertical) that cause error in the gravity anomaly estimation. The first one is defined by the first term of formula 1.3.11. This error has a cosine (quadratic for small stabilization error angles) nature and does not impose any strict requirements on the accuracy of keeping the GSE sensitive axis vertical. It is easy to show that in this case, the error in keeping the GSE sensitive axis vertical equal to 4.5 arcmin leads to an error in the gravity anomaly estimation equal to 1 mGal. Much stricter requirements for the GSE sensitive axis vertical alignment are imposed by the effect of horizontal accelerations on the GSE sensitive axis, defined by the second and third terms of formula (1.3.11). Let us estimate the influence of this error component on the gravimeter error. Assume that the aircraft or, more precisely, the place where the GSE proof mass is located on it, performs harmonic motion in the horizontal plane with amplitude of 25 m and a period of 100 s. Let the error in keeping misalignment errors of GSE sensitive axis be 10 arcsec. Then it is easy to show that the amplitude of the gravity anomaly generation error due to the projection of the horizontal acceleration onto the GSE sensitivity axis will be 0.5 mGal. Therefore, the requirement for the error in keeping the GSE sensitive axis vertical in airborne gravimetry is from 10 to 15 arcsec.

A similar result was also obtained using real data of horizontal accelerations from ten survey lines in different flight conditions. For this purpose, horizontal accelerations were scaled and passed through a filter with an averaging time of 100 s. The following conclusion was made based on the calculation results: the accuracy required to maintain (know) the GSE sensitive axis vertical deflection angles for airborne gravimetry of the 0.5 mGal level is from 10 arcsec in favorable flight conditions to 6 arcsec in adverse flight conditions.

The error in keeping the GSE sensitive axis vertical depends on two components: instability of the angles β_Z, γ_Z between the GSE sensitive axis and the normal to the plane of the platform due to the instability of zero drifts of horizontal accelerometers (see the explanations for formula 1.3.1) and errors in determining the gyro platform angles α_1, α_2 during the flight.

To reduce the influence of the first component of the error, the "Autocalibration" procedure was introduced in the software of the GT-2A gravimeter which helps occasionally, once every 10–15 days and after each cold start of the gravimeter, determine the estimates $\hat{\beta}_Z$, $\hat{\gamma}_Z$. Certain values $\hat{\beta}_Z$, $\hat{\gamma}_Z$ are entered into the database of the gravimeter and taken into account in real time to form corrections in accordance with the second and third terms of formula 1.3.11. The second component of α_1, α_2 is determined during postprocessing in the GTNAV software (see Sect. 1.2.2). Errors in determining the sum of the components $\beta_Z + \alpha_1$, $\gamma_Z + \alpha_2$ are additionally estimated by the correlation method at the postprocessing stage in the GTRAV software. These solutions provide the required accuracy of keeping the GSE sensitive axis vertical.

Nonorthogonality of the DTG angular momentum with respect to the gyro platform plane. Consider a simple example (Fig. 1.33) explaining the disturbance of a gyro platform placed in a biaxial gimbal suspension during its azimuthal turn.

Figure 1.33 represents one axis of a biaxial gyrostabilizer. As mentioned above, the plane of the platform is a conventional concept; it is defined by accelerometer signals. The top part of the figure shows the gyro platform with its plane in the horizontal position, an accelerometer signal, which is conventionally represented as a spring ball and has zero readings. If the gravimeter is quickly rotated by 180° around its vertical axis, the position of the angular momentum in the inertial space will remain unchanged at the first moment of time (it can be assumed that under

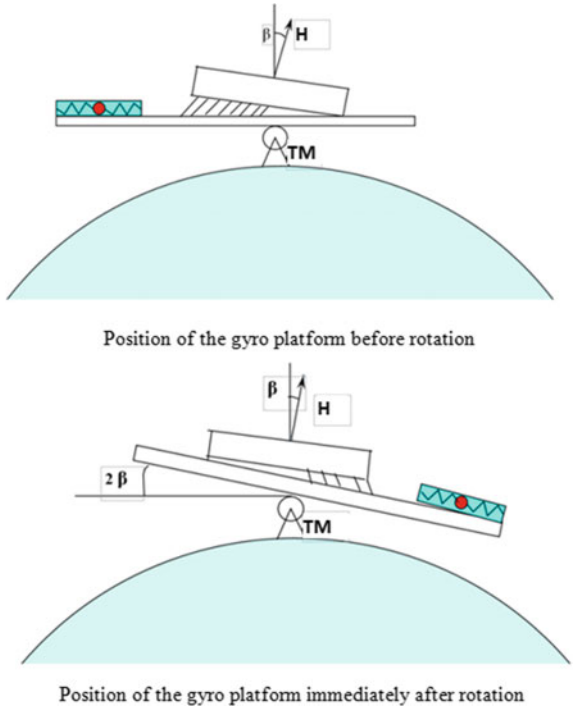

Fig. 1.33 The error in the alignment of the DTG angular momentum orthogonally to the platform plane

the influence of the correction system, the gyroscope precession can be neglected). As a result, at the first moment, the platform will deviate from the horizon plane by an angle of 2 β, which will be measured by the accelerometer, where β is the nonorthogonality angle of the gyroscope angular momentum to the platform plane.

This effect served as a basis for the method of determining nonorthogonality of the DTG angular momentum vector of the platform plane at the manufacturing instrument making plant. After determining the angles β (rotation around the X axis) and γ (rotation around the Y axis), the angular momentum vector is vertically aligned by adding the constants $\widehat{dw}_x = g\beta$ and $\widehat{dw}_y = -g\gamma$ to the signals of the accelerometers X and Y, respectively.

During operation, the DTG angular momentum deviates from the normal to the platform plane due to the instability of the accelerometer zero signals (for A15 accelerometers used in the gravimeter, the instability of zero signals is estimated at a level of ±10 arcsec). To ensure that this error does not cause the platform deviation from the horizon plane during the vehicle maneuvers, the third external azimuthal axis is used to stabilize the gravimeter (platform) position in the geographic coordinate system. Thus, the use of the third azimuthal axis completely eliminates the gravimeter error caused by the nonorthogonality of the DTG angular momentum of the gyro platform plane.

It is easy to show that the use of the third axis, which allows gyro platform stabilization in the geographic reference frame, also eliminates the effect of the constant components of the estimation errors of the scale factors and drifts of the DTG channels on the angular errors of the gyro platform.

1.3.6 Main Tasks of the Gravimeter Central Processing Unit

The central device is designed to generate preliminary (raw) gravimetric data. Its CPU executes the following relevant tasks.

Gravimeter startup. After the gravimeter is switched on, relevant gravimeter systems start their operation automatically according to the time diagram.

Generation of input data. At a frequency of 300 Hz, the data acquisition system forms information read out from the DTG angle sensors, GSE, accelerometers QAx, QAy, the FOG, and the GSE position sensor. GSE readings are corrected for the Harisson effect (according to signals from the DTG angle sensors), nonorthogonality of the GSE sensitive axis to the platform plane (according to the QAx, QAy readings), and the influence of the squares of horizontal accelerations.

Control of stabilization servo drives. The task generates the signals applied to the torque sensors DM_x, DM_y of the horizontal axes of the gimbal suspension and the azimuth stabilization motor. The task of horizontal stabilization servo drives implemented as a discrete Kalman filter operates at a frequency of 300 Hz. The input data are signals from QA accelerometers (to provide an intermediate stage for gravimeter startup) or from DTG angle sensors read out in the normal operation

mode. The input data for the control of the azimuth servo drive is the generated value of the compass heading of the gyro platform.

Systems for correcting gyro platform attitude. The task provides a proportional correction in the gravimeter startup mode and a Schuler-type integral correction in the operating mode. The input data for the task are the signals of the QAx, QAy accelerometers, the FOG, and data on the latitude and the vehicle vector velocity from the GNSS receiver.

Calculation of the compass heading of the gyro platform. The task calculates the geographical heading of the gyro platform, which is the input for the task of control of the gravimeter azimuthal servo system. The task input data are the values of the absolute angular rates of the platform obtained in the previous task, as well as the data on the GNSS-derived velocity.

Generation of the vehicle attitude angles. The task generates the heading, the angles of roll and pitch of the aircraft based on the data obtained from the previous task, as well as the readings of the stabilization angle sensors. The angles of roll and pitch are used in postprocessing to recalculate the coordinates of the GNSS antenna to the GSE location.

Gravimetric data generation. The task generates three suboptimal estimates of the gravity anomalies with various averaging times in real time (for more details, see Sect. 2.4). In addition, in the marine version, the task generates a mean value of the vertical specific acceleration per second which, at the customer's request, can be transferred to their data acquisition system. In the airborne version of the gravimeter, the generated value of the gravity anomaly is used to control the GSE on a fixed platform and to estimate the noise level of the output information of the gravimeter.

Thermal regulation. The task ensures generation of signals for the triggering the thermal regulation system (heaters and fans). The task input is signals from the thermal sensors.

Reception of commands and data output. The task ensures interaction of the computing unit of the central device with the computing unit of the control and indication device (CID). In the airborne version, during a gravity survey, the task ensures the generation of data for two so-called S- and G-files. The S-file contains information on the dynamics of the gravimeter gyro horizon; it is recorded on the CID hard disk with a frequency of 3 Hz, and serves as input information for the optimal filter implemented in the GTNAV software, which evaluates the disturbed state of the gravimeter gyro horizon in postprocessing. The G-file contains information with a frequency of 18 Hz on the measured values of the vertical and horizontal specific forces; it is recorded on the CID hard disk and used in the postprocessing task of GTGRAV software to generate gravity anomalies on the aircraft flight trajectory. For details, see Sect. 2.2.

In the marine version, the CID receives data on the three gravity anomaly values with various averaging times from the CPU in real time and records them into the G file on the hard disk once every 10 s.

Autocalibration. The task is executed occasionally during the gravimeter operation. It determines the estimates of the deviation angles $\hat{\beta}_Z$, $\hat{\gamma}_Z$ of the GSE sensitive axis from the normal to the plane of the platform by the method of successive tilts

of the platform around the X, Y axes at known fixed angles determined by QAs. At the same time, estimates of the FOG drift $\widehat{dr}$ and the drift components of the DTG gyroscope $\widehat{dp}$, $\widehat{dq}$ are determined by the method of successive rotation of the platform at 0° and 270° rhumbs. After the task is completed, the resulting parameter values are entered into the gravimeter database in order to enter corrections in real time. The task runs 5.5 h.

Calibration. Calibration is performed at the instrument making plant during the gravimeter manufacturing. It automatically determines the estimates of the deviation angles $\hat{\beta}_Z$, $\hat{\gamma}_Z$ of the GSE sensitive axis from the normal to the plane of the platform by the method of successive tilts of the platform around the X, Y axes at known fixed angles determined by QAs. At the same time, the thickness of leveling shims for the GSE base is calculated to eliminate the specified deviation. The duration of this task is 3 h.

Monitoring of the gravimeter state. The extensive monitoring system allows efficient diagnostics and timely detection of faults arising during operation. The task forms two generalized criteria of the state (readiness of the gravimeter):

- the gravimeter is serviceable (yes/no): hardware serviceability;
- g is reliable (yes/no): the reliability of measurements.

The gravimeter hardware serviceability criterion is generated as a logical sum of twenty fault criteria of elements and systems recorded in a special CID control frame.

The display of the CID monitor shows fault symptoms from the first fault detection until the operator issues the Fault Accepted command. If a fault symptom is not removed, that means that it is present at the time of issuing the command. Thus, no short-term fault goes unnoticed by the operator.

The criterion of the reliability of measurements is formed as a logical sum of six criteria such as the increased turbulence, the lack of information from the GNSS for more than 10 min during which the damping of the gyro platform oscillations is disabled, and other such criteria. In the CID frame, the operator observes the generalized criteria of the gravimeter state, and only if the gravimeter fault or unreliable measurements are detected, he turns to monitoring to find out the reasons.

Based on the results of the monitoring, a status word is generated which is recorded to the output G- and S-files.

To make fault diagnostics easier, the CPU forms diagnostic data during the operation of the gravimeter, and the CID records the so-called diagnostic file on its hard disk, which allows for remote fault diagnostics.

Noise level assessment. The task assesses the quality of the gravimeter operation on a fixed base. The task input is the output of the task on generation of gravimetric information. The task of assessing the noise level simulates the initial and final reference measurements with a length of 15 min and a flight with a length of 3 h. According to the results of the reference measurements, the simulated flight measurements are adjusted and the standard deviations of measurement errors are calculated. The result is displayed on the CID monitor.

1.3.7 Conclusions

The features of the GT-2 gravimeters have been considered both in terms of their design and software. Extremely stringent accuracy requirements for subsystems of the airborne gravimeter have been formulated; the proposed hardware, firmware, and software solutions have made it possible to satisfy the above requirements. The accuracy parameters, as well as the operational features including, in particular, the presence of a gyro platform which remains undisturbed during vehicle maneuvers, a wide dynamic measurement range (± 1 g) and a small GSE drift (3 mGal/month) have determined a great interest of Russian and international companies in gravimeters of this series.

References

Arias F, Jiang Z, Robertsson L, Vitushkin L et al (2012) Final report of key comparison CCM. G-K1: International comparison of absolute gravimeters ICAG2009. Metrologia 49(1A), Tech Suppl 07011

Arnautov GP, Gik LD, Kalish EN, Koronkevich VP, Malyshev IS, Nesterikhin YuE, Stus YuF, Tarasov GG (1974) High-precision laser gravimeter. Appl Opt 13(2):310–313

Arnautov GP, Kalish EN, Smirnov MG, Stus YuF, Tarasyuk VG (1988) Ballistic gravimeter. Author's Certificate SSSR SU 1563432, G 01 V 7/14, 01/08/1988

Atakov AI, Lokshin BS, Prudnikov AN, Shkatov MY (2010) Results of integrated geophysical survey at the Ushakovsko-Novosemel'skaya prospective area in the Kara Sea. In: IAG symposium on terrestrial gravimetry: static and mobile measurements (TG-SMM2010). Elektropribor, St. Petersburg, pp 33–35

Barthelmes F, Petrovic S, Pflug H (2013) First experiences with the GFZ new mobile gravimeter Chekan-AM, Paper abstracts of IAG symposium on terrestrial gravimetry: static and mobile measurements (TG-SMM2013). Elektropribor, St. Petersburg, p 18

Baumann H, Klingele EE, Marson I (2012) Absolute airborne gravimetry: a feasibility study. Geophysical prospecting, March 2012, pp 361–372

Berezin VB, Berezin VV, Tsitsulin AK, Sokolov AV (2004) Adaptive image reading in an astronomical system on a matrix CCD. Izvestiya vysshykh uchebnykh zavedenii, Radioelektronika 4:36–45

Berzhitsky VN, Ilyin VN, Smoller YL, Yurist SS (1999) Analog-to-digital converter. Patent of the Russian Federation no. 2168269 dated 12/23/1999

Berzhitsky VN, Ilyin VN, Smoller YL, Cherepanov VA, Yurist SS (2000) Three-axis gyrostabilizer. Patent of the Russian Federation no. 2157966 dated 01/17/2000

Berzhitsky VN, Bolotin YV, Golovan AA, Iljin VN, Parusnikov NA, Smoller YL, Yurist SS (2002) GT-1A inertial gravimeter system. Results of flight tests. Center of Applied Research Publishing House, Faculty of mechanics and mathematics, Moscow State University, Moscow

Bikeeva MM, Smirnova LA, Sokolov AV (2007) Features of the geophysical studies using a marine gravimetric system. In: 8 konferentsiya molodykh uchenykh Navigatsiya i upravlenie dvizheniem (8th Conference of Young Scientists Navigation and Motion Control). Elektropribor, St. Petersburg, pp 162–167

Blazhnov BA, Nesenyuk LP, Elinson LS (1994) Eliminating the effect of gravitational field smoothing in processing the readings of a damped airborne gravimeter. In: Proceedings of the international conference shipborne and airborne gravimetry 94, St. Petersburg

Blazhnov BA, Nesenyuk LP, Peshekhonov VG, Sokolov AV, Elinson LS, Zheleznyak LK (2002) Integrated mobile gravimetric system: development and test results. In: Volfson GB, Peshekhonov VG (eds), Primenenie graviinertsial'nykh tekhnologii v geofizike (Application of Graviinertial Technologies in Geophysics), St. Petersburg, pp 33–44

Boedecker G (2002) World gravity standards—present status and future challenges. Metrologia 39(5):429–433

Bordé CJ (2002) Atomic clocks and inertial sensors. Metrologia 39(5):435–463

Bronshtein IG, Livshits IL, Elinson LS, Gerasimova NL, Sokolov AV (2001) Quartz Gravimeter: Patent no. 2171481 of the Russian Federation: MPK G01V7/02/ appl 03.02.2000; pub 27/07/2001

Canuteson EL, Zumberge MA (1996) Fiber-optic extrinsic Fabry-Perot vibration isolated interferometer for use in absolute gravity meters. Appl Opt 35(19):3500–3505

Chelpanov IB, Nesenyuk LP, Braginsky MV (1978) Raschet kharakteristik navigatsionnykh giropriborov (Calculation of Characteristics of Navigation Gyrodevices). Sudostroenie, Leningrad

Cook AH (1965) The absolute determination of the acceleration due to gravity. Metrologia 1(3):84–114

Crossley D, Vitushkin LF, Wilmes H (2013) Global reference system for determination of the Earth gravity field: from the Potsdam system to the Global Geodynamics Project and further to the international system of fundamental absolute gravity stations. Trudy Instituta Prikladnoi Astronomii RAN 27:333–338

Dehlinger P (1978) Marine gravity, Amsterdam

Drobyshev NV, Koneshov VN, Koneshov IV, Solov'ev VN (2011) Development of an aircraft laboratory and a procedure for airborne gravimetric surveys in Arctic conditions, Vestnik Permskogo universiteta, Geologiya Series, no 3, pp 37–50

Forsberg R, Olesen A, Einarsson I (2013) Airborne gravimetry for geoid determination with Lacoste Romberg and Chekan gravimeters. In: IAG symposium on terrestrial gravimetry: static and mobile measurements (TG-SMM2013). Elektropribor, St. Petersburg, pp 22–28

Francis O, Baumann H, Volarik T, Rothleitner C (2014) The European comparison of absolute gravimeters 2011 (ECAG-2011) in Walferdange, Luxembourg: Results and recommendations. Metrologia 50(3):257–268

Francis O, Baumann H, Ullrich C et al (2015) CCM. G-K2 key comparison. Metrologia 52(1A) Tech Suppl 07009

Germak A, Desogus S, Origlia C (2002) Interferometer for the IMGC rise-and-fall absolute gravimeter. Metrologia 39(5):471–475

Gillot P, Francis O, Landragin A, Pereira Dos Santos F, Merlet S (2014) Stability comparison of two gravimeters: optical versus atomic interferometers. Metrologia 51(5):L15–L17

Ilyin VN, Volnyansky VN, Nikitin VP, Smoller YL, Yurist SS (1993) Gravimeter for measuring gravity from moving vehicles. Patent of the Russian Federation No. 2056643 dated 07/09/1993

Jiang Z, Pálinkáš V, Arias FE, Liard J, Meriet S, Vitushkin L et al (2012) The 8th international comparison of absolute gravimeters 2009: The first key comparison (CCM.GK1) in the field of absolute gravimetry. Metrologia 49(6):666–684

Koneshov VN, Bolotin YV, Golovan AA, Smoller YL, Yurist SS, Fedorova IP, Hevison W, Richter T, Greenbaum J, Young D, Blankenship D (2013a) Using airborne gravimeter GT-2A in polar areas. In: IAG symposium on terrestrial gravimetry: static and mobile measurements (TG-SMM2013a). Elektropribor, St. Petersburg, pp 36–40

Koneshov VN, Koneshov IV, Klevtsov VV, Makushin AV, Smoller YL, Yurist SS, Bolotin YV, Golovan AA (2013b) An approach to refined mapping of the anomalous gravity field in the Earth's polar caps. Izvestiya, Phys Solid Earth 49(1)):77–79

Koneshov VN, Nepoklonov VB, Sermyagin RA, Lidovskaya EA (2013c) Modern global Earth's gravity field models and their errors. Gyroscopy Navig 4(3):147–155

Kontarovich RS (2015) Aerogeophysica Inc Company: 45 years in service of the national geology. Razvedka i okhrana nedr 12:3–6

Kontarovich RS, Babayants PS (2011) Airborne geophysics: An effective tool to solve geological prospecting problems. Razvedka i okhrana nedr 7:3–7

Kovrizhnykh PN, Shagirov BB (2013) Marine gravity survey of the Kazakhstan sector of the Caspian Sea. In: IAG symposium on terrestrial gravimetry: static and mobile measurements (TG-SMM2013). Elektropribor, St. Petersburg, pp 59–62

Kovrizhnykh PN, Shagirov BB, Zhunusov IE, Saurykov ZZ (2013a) Gravity surveys in the Caspian Sea Kazakhstan transition zone. In: IAG symposium on terrestrial gravimetry: static and mobile measurements (TG-SMM2013). Elektropribor, St. Petersburg, pp 73–76

Kovrizhnykh PN, Shagirov BB, Yurist SS, Bolotin YV, Saurykov Z, Karsenov T et al. (2013b) Marine surveys in the Caspian Sea using GT-2M, Chekan-AM and LR gravimeters: accuracy comparison. Geol Protect Mineral Resour 4:58–62

Kovrizhnykh PN, Saurykov ZZ, Shagirov BB, Paydin MO (2016) Experience of airborne gravimetric surveys in Kazakhstan upland conditions. In: 4th IAG symposium on terrestrial gravimetry: static and mobile measurements (TG-SMM2016). Elektropribor, St. Petersburg, pp 44–52

Krasnov AA (2007) Results of bench and field tests of the airborne gravimeter gyrostabilizer. In: 9 konferentsiya molodykh uchenykh "Navigatsiya i upravlenie dvizheniem" (9th Conference of Young Scientists "Navigation and Motion Control"). Elektropribor, St. Petersburg, pp 26–33

Krasnov AA, Sokolov AV (2009) Development and implementation of airborne gravimetric measurement processing methods. In: Materialy X konferentsii molodykh uchenykh "Navigatsiya i upravlenie dvizheniem" (10th Conference of Young Scientists "Navigation and Motion Control"). Concern CSRI Elektropribor, St. Petersburg

Krasnov AA, Odintsov AA, Semenov IV (2010) Gyro stabilization system of a gravimeter. Gyroscopy and Navigation 1:191–200

Krasnov AA, Sokolov AV, Elinson LS (2014a) Operational experience with the Chekan-AM gravimeters. Gyroscopy Navig 5(3):179–183

Krasnov AA, Sokolov AV, Elinson LS (2014b) A new air-sea shelf gravimeter of the Chekan series. Gyroscopy Navig 5(3):129–135

Krasnov AA, Sokolov AV, Evstifeev MI, Starosel'tseva IM, Elinson LS, Zheleznyak LK, Koneshov VN (2014c) A new generation of gravimetric sensors. Meas Tech 57(9):967–972

Lygin VA (2010) Gravity surveys in transition zones with the use of hovercraft. In: IAG symposium on terrestrial gravimetry: static and mobile measurements (TG-SMM2010). Elektropribor, St. Petersburg, pp 47–49

Logozinsky VN, Solomatin VA (1996) Fiber-optic gyroscopes for industrial use. Giroskopiya i Navigatsiya 4:27–31

Matveev VA, Podchezertsev VP, Fateev VV (2005) Giroskopicheskie stabilizatory na dinamicheski nastraivaemykh giroskopakh (Gyroscopic Stabilizers on Dynamically Tuned Gyroscopes). MGTU im. N.E. Baumana, Moscow

Merlet S, Gouët JL, Bodart Q, Clairon A, Landragin A, Pereira dos Santos F, Rouchon P (2009) Operating an atom interferometer beyond its linear range. Metrologia 46(1):87–94

Mogilevsky VE, Kontarovich OR (2011) Airborne gravimetry: an innovative technology in geophysics. Razvedka i okhrana nedr 7:7–10

Mogilevsky VE, Kaplun DV, Kontarovich OR, Pavlov SA (2010) Airborne gravity surveys in Aerogeophysica Inc. In: IAG symposium on terrestrial gravimetry: static and mobile measurements (TG-SMM2010). Elektropribor, St. Petersburg, pp 42–46

Mogilevsky VE, Pavlov SA, Kontarovich OR, Brovkin GI (2015a) Features of airborne geophysical surveys in high latitudes. Razvedka i okhrana nedr 12:6–10

Mogilevsky VE, Brovkin GI, Kontarovich OR (2015b) Accomplishments, features, and problems of airborne gravimetry. Razvedka i okhrana nedr 12:16–25

Nesenyuk LP, Elinson LS (1995) The experience in carrying out a detailed marine gravimetric survey. Giroskopiya i Navigatsiya 4:60–67

Niebauer TM, Hollander WJ, Faller JE (1994) Absolute gravity in-line measuring apparatus incorporating improved operating features, United States Patent #5,351,122, Sept 27, 1994

Niebauer TM, Sasagawa GS, Faller JE, Hilt R, Klopping F (1995) A new generation of absolute gravimeters. Metrologia 32(3):159–180

Orlov OA, Vitushkin LF (2010) A compact green laser for absolute ballistic gravimeter. In: IAG symposium on terrestrial gravimetry: static and mobile measurements (TG-SMM2010). Elektropribor, St. Petersburg

Panteleev VL (1983) Osnovy morskoi gravimetrii (Fundamentals of Marine Gravimetry). Nedra, Moscow

Pamyati professora L.P. Nesenyuka (2010) Izbrannye trudy i vospominaniya (In Memory of Professor L.P. Nesenyuk. Selected Papers and Memoirs). CSRI Elektropribor, St. Petersburg

Peshekhonov VG, Sokolov AV, Elinson LS, Krasnov AA (2015) A new air-sea gravimeter: development and test results. In: 12th St. Petersburg international conference on integrated navigation systems. Elektropribor, St. Petersburg, pp 173–179

Peshekhonov VG, Sokolov AV, Zheleznyak LK, Bereza AD, Krasnov AA (2020) Role of navigation technologies in mobile gravimeters development. Gyroscopy Navig 11(1):2–12

Peters A, Chung KY, Chu S (2001) High-precision gravity measurements using atom interferometry. Metrologia 38:25–61

Popov EI (1959) Quartz gravimeter for marine observations. Trudy IFZ AN SSSR (Trans of the Institute of Physics of the Earth of The Russian Academy of Sciences) 8:32–41

Richter TG, Greenbaum JS, Young DA, Blankenship DD, Hewison WQ, Tuckett H (2013) University of Texas airborne gravimetry in Antarctica, 2008 to 2013. In: Paper abstracts of IAG symposium on terrestrial gravimetry: static and mobile measurements (TG-SMM2013). Elektropribor, St. Petersburg, p 13

Seleznev VP (1967) Navigatsionnye ustroistva (Navigation Devices). Oborongiz, Moscow

Smoller YL (2002) Mechanics, control and processing algorithms in the inertial-gravimetric aerial complex. Cand Sci Dissertation, Moscow

Smoller YL, Yurist SS, Fedorova IP, Bolotin YV, Golovan AA, Koneshov VN, Hevison W, Richter T, Greenbaum J, Young D, Blankenship D (2013) Using airborne gravimeter GT-2A in polar areas. In: IAG symposium on terrestrial gravimetry: static and mobile measurements (TG-SMM2013). Elektropribor, St. Petersburg, pp 36–40

Smoller YL, Yurist SS, Golovan AA, Yakushik LY (2015) Using a multiantenna GPS receiver in the airborne gravimeter GT-2a for surveys in polar areas. Gyroscopy Navig 6(4):299–304

Smoller YL, Yurist SS, Golovan AA, Iakushyk LY, Hewison YW (2016) Using quasicoordinates in software of multi-antenna GPS receivers and airborne gravimeter GT-2A for surveys in Polar Areas, In: 4th IAG symposium on terrestrial gravimetry: static and mobile measurements (TG-SMM2016). Elektropribor, St. Petersburg

Sokolov AV (2003) Mobile gravimeter. Prib Tekh Eksp 46(1):165–166

Sokolov AV, Usov SV, Elinson LS (2000) The experience of conducting gravity surveys in the conditions of marine seismic operations. Giroskopiya I navigatsiya 1:39–50

Sokolov AV (2004) Evaluating the position of the optical signal of a known shape. In: 6 konferentsiya molodykh uchenykh "Navigatsiya i upravlenie dvizheniem" (6th Conference of Young Scientists "Navigation and Motion Control"). Elektropribor, St. Petersburg, pp 248–254

Sokolov AV, Krasnov AA, Elinson LS, Vasil'ev VA, Zheleznyak LK (2015) Calibration of the Chekan-AM gravimeter by a tilting method. Gyroscopy Navig 6(4):288–293

Sokolov AV, Krasnov AA, Alekseenko AS, Stus YF, Nazarov EO, Sizikov IS (2017) Measuring absolute gravity aboard moving vehicles. Gyroscopy Navig 8(4):287–294

Sokolov AV, Staroseltseva IM, Elinson LS (2008) Gravity measurement device: Pat. No. 2377611 Russian Federation: IPC G01V7/00/appl. 04/22/2008; pub. 12/27/2009

Sokolov AV, Krasnov AA, Konovalov AB (2021) Automation of mobile gravimeter quartz elastic system manufacturing technology. Gyroscopy Navig 12(2):138–146

Vitouchkine AL, Faller JE (2002) Measurement results with a small cam-driven absolute gravimeter. Metrologia 39(2):465–469

Vitushkin LF (2011) Measurement standards in gravimetry. Gyroscopy Navig 2(3):184–191

Vitushkin LF, Orlov OA (2011) Absolute ballistic gravimeter. Patent for invention no. 2475786, May 06, 2011

Vitushkin LF, Orlov OA (2014) Absolute ballistic gravimeter ABG-VNIIM-1 developed at D.I. Mendeleev Research Institute for Metrology. Giroskopiya i navigatsiya 2:95–100

Vitushkin LF, Orlov OA, Germak A, D'Agostino G (2012) Laser displacement interferometers with subnanometer resolution in absolute ballistic gravimeters. Meas Tech 55(3):221–228

Zheleznyak LK, Popov EI (1982) Principles of construction and optimal design of a modern marine gravimeter. In: Fiziko-tekhnicheskaya gravimetriya (Physical and Technical Gravimetry). Nauka, Moscow, pp 43–60

Zheleznyak LK, Popov EI (1984) Uprugaya sistema tipa USG. Pribory i metody obrabotki gravi-inertsial'nykh izmerenii (Elastic system of the gravimeter. Devices and methods for processing graviinertial measurements). IFZ, AN SSSR, Moscow, pp 54–66

Zheleznyak LK, Markov GS, Romanishin PA (1983) Experimental production gravimetric survey in the Black Sea. In: Graviinertsial'nye issledovaniya (Gravi-Inertial Studies). IFZ AN SSSR, Moscow, pp 35–42